Role of Flow Alignment and Inlet Blockage on Vaned Diffuser Performance

by

Michael S. Phillips

GTL Report #229 September 1997

GAS TURBINE LABORATORY
MASSACHUSETTS INSTITUTE OF TECHNOLOGY
CAMBRIDGE, MASSACHUSETTS

Role of Flow Alignment and Inlet Blockage on Vaned Diffuser Performance

by

Michael S. Phillips

GTL Report #229 September 1997

This research was sponsored by the Army Research Office, Dr. Thomas Doligalski, Technical Monitor. Additional funding was provided by NASA Lewis Research Center, AlliedSignal Inc., and IHI Toyosu.

Role of Flow Alignment and Inlet Blockage on Vaned Diffuser Performance

by

MICHAEL STEPHEN PHILLIPS

Abstract

A computational investigation of the effects of inlet conditions on straight-channel diffuser performance is undertaken. The steady, three-dimensional, Navier-Stokes solver used for the investigation is found to adequately model the performance of a diffuser that has been previously examined experimentally.

Results indicate that, contrary to the established view, vaned diffuser channel performance is weakly dependent on throat blockage. Rather, channel pressure rise is strongly affected by flow angle alignment with the diffuser centerline; misalignment of the flow can cause separation and reduced channel performance. This result challenges current design methods, and indicates that the designer is capable of sculpting the diffuser vanes to change the flow angle alignment, thus enabling control of both performance and range.

In support of experimental results, overall diffuser performance is found to be largely independent of inlet axial distortion. Inlet nonuniformities are attenuated within the diffuser channel due to a spanwise work transfer which energizes regions of high flow angle misalignment, thus preventing the development of localized channel stall, and preserving good diffuser performance. This result indicates that axially twisted vanes, which are tailored for nonuniform inlet flow, may be unnecessary; simple untwisted vanes display no loss of performance when subjected to severe inlet distortion.

Acknowledgments

This research was funded by Army Research Organization Grant # DAAH04-93-G-0394, with Dr. Thomas Doligalski acting as Technical Monitor. Additional funding was provided by the NASA Lewis Research Center (NAG3-1598; Dr. D.R. Reddy, Technical Monitor), Allied Signal Inc. (P.O. E391868; Dr. Arun Sehra, Technical Monitor), and IHI Toyosu (research agreement; Mr. Hideaki Tamaki, Technical Monitor).

I would like to thank my advisor, Dr. Choon S. Tan, for taking me under his wing. Dr. Tan's dedication to my understanding and his faith in my abilities deserves my total gratitude. Thanks, Choon.

I am indebted to Dr. Sabris Deniz, who's research and helpful discussions form the backbone of my knowledge of centrifugal diffusers. Professor Edward Greitzer always kept me focused on the problem at hand, and taught me the intricacies of internal flows. Professor William Dawes and Professor Nicholas Cumpsty of the University of Cambridge provided invaluable advice on the numerical code and fluid mechanics issues. Post-processing was performed using Professor Jaime Peraire's FELISA and Bob Haimes's VISUAL3.

Fellow student Patrick Shum selflessly assisted me with NEWT, FORTRAN, and pre/post-processing. Takeo Kuraishi and Dr. Ted Valkov provided essential computer management. Steven Lukatchko, Sonia Ensenat, and Amit Mehra introduced me to VISUAL3.

A large part of my success at MIT has been due to those angels who have watched over my sanity. My parents are my two heroes who without exception have *always* been there for me, and have supported me in every crazy goal I have ever pursued. My brother Bob ('87) [27], as well as Michele, Trisch, and Dave have left me some enormous shoes to fill, but continue to provide all the love and support I need to grow into them. Thanks to my close friends in the GTL, as well as around Boston and throughout the world, who've kept me laughing, and have given me countless stories I wouldn't dare tell my grandkids ;-)

MIT can sometimes be an unreasonable place, where nearly everything you ever held passion for is sacrificed and replaced by an unshakeable focus on research and academia. Thanks to family and friends for always reminding me that the world is so much larger and that the true treasures are so much greater. Now it is time to explore!

Contents

Nomenclature

Variables

A	Area
A_{eff}	Effective Flow Area
A_{geo}	Geometric Flow Area
AR	Area Ratio (Exit/Throat)
AS	Throat Aspect Ratio (b/W_{th})
b	Spanwise (Axial) Distance
B	Blockage
Cp	Pressure Recovery
L	Channel Length
LWR	Length-to-Width Ratio
$\dot{m}$	Mass Flow Rate
M	Mach Number
N_v	Vane Number
P	Pressure, Static Quantity
R	Radial Distance
T	Temperature, Static Quantity
V	Velocity
W_{th}	Throat Width
α	Flow Angle (Measured from Radial)
α_v	Geometric Inlet Angle

β_v	Vane Wedge Angle
γ	Specific Heat Ratio
ρ	Density
$\Re$	Gas Constant for Air
2θ	Vane Divergence Angle

Subscripts

r	Radial Component
θ	Tangential Component
z	Axial Component
m	Meridional Component (Along Diffuser Centerline)
T	Stagnation Quantity
1	Diffuser Inlet
th	Diffuser Throat Plane
2	Diffuser Exit
$1-2$	Overall Diffuser
$1-th$	Semi-Vaneless Region
$th-2$	Channel Region

Superscripts

$\hat{}$	Mass-Averaged Value
Ψ	Availability-Averaged Value

Chapter 1

Introduction

1.1 Centrifugal Compressor History

Historically, centrifugal compressors have received limited attention within the aircraft engine industry. Axial flow machines have been favored because of their high mass flow and high efficiency capabilities, while radial pumps have been limited to smaller, less demanding applications such as commercial vacuum cleaners, air conditioning units, and automobile turbochargers [18].

However, the advantages of the radial machine are numerous; the device is cheaper, more reliable, has fewer parts, and produces higher stage pressure ratios than its axial counterpart. Unfortunately, complex three-dimensional unsteady flow within the centrifugal stage currently results in high losses, although it is believed that increased investigation into the fluid mechanics of the device could inspire designs with significantly improved efficiency [32].

1.2 Description of the Radial Compressor

The centrifugal compressor stage consists of a rotating impeller and a stationary diffuser, as shown in Figure 1-1. The impeller adds kinetic energy to the flow, and the downstream diffuser must decelerate the flow and convert kinetic energy into static pressure recovery.

In high performance applications, the diffuser can be the critical component in establishing stage efficiency and pressure rise [18, 26].

Radial diffusers can be classified as passage and vaneless diffusers. Vaneless diffusers are simple to design and offer satisfactory performance over a large flow range. Passage diffusers are considerably more complex, yet are able to provide high performance and efficiency over a narrow flow range. Current and future design trends indicate a need for both high efficiency and wide flow range, a combination possible only with passage diffusers [11]. For this reason, centrifugal compressors with passage diffusers are receiving more attention from both industry and research organizations.

A large number of radial passage diffuser designs have been developed utilizing simple wedges, plates, airfoil cascades, and conical pathways; Figure 1-2 shows a sample of the diffuser designs available. All of these diffusers operate by using a vane geometry to convert angular momentum of the impeller exit flow into static pressure rise; therefore, they are often called vaned diffusers. The performance and flow range of these diffusers are arguably similar [11], and the disagreement over optimum design demonstrates the lack of understanding of the complex fluid mechanics occurring in these devices.

Of the wide variety of vaned diffusers, the straight-channel diffuser represents the simplest design from a manufacturing viewpoint, and is the most common passage diffuser in use today [12]. Traditionally, the straight-channel diffuser has been designed by utilizing the substantial database of single-element, two-dimensional, straight-walled laboratory diffuser data (see Section 4.1.2 for an overview of diffuser design methodology). Again, the performance of the straight-channel diffuser is quite similar to other passage geometries, and it is assumed that any insight gained through studies of the straight-channel diffuser can be applied to all vaned geometries.

1.3 Background in Radial Diffuser Research

While the investigation of centrifugal compressors lags behind axial compressor research, significant contributions to the field have been made. A very brief literature review is

provided below, and more exhaustive reviews can be found in Deniz [11] and Cumpsty [3].

1.3.1 Important Research Accomplishments

Early diffuser design was traditionally based on an assumption of steady, axisymmetric flow leaving the impeller and entering the diffuser. Dean & Senoo [10] first proposed a nonuniform jet-wake model for vaneless diffuser inlet flow, and suggested that nonuniformity can affect flow behavior. With the advent of laser flow visualization techniques, more information about the impeller exit flow field became available. Eckardt [16] and Krain [24] observed strong distortion in both the circumferential and axial directions, continuing from the impeller exit into the diffuser inlet and throat; Figure 1-3 shows a velocity wake present at the shroud-suction side corner of the impeller exit, taken from Eckardt [16]. Cumpsty [3] and Dawes [5] provided evidence that axial nonuniformity present at the diffuser inlet influences performance much more than circumferential distortion. Other researchers (see Section 1.3.2) have reached opposing conclusions.

Recent advances in numerical solvers and increased computational resources have allowed computational fluid dynamics (CFD) to become a practical research tool. Dalbert et al. [4] applied a steady, three-dimensional, Navier-Stokes solver to a vaned diffuser geometry, and demonstrated the ability of CFD to capture complicated flow phenomena which are not revealed experimentally by traditional wall pressure taps and wall streamline visualization. Dawes [5] demonstrated the use of an unsteady, three-dimensional, Navier-Stokes solver in predicting the performance of an impeller-diffuser stage.

1.3.2 A Brief Review of MIT Swirl Generator Studies

A swirling-radial-flow generator was developed at MIT by Filipenco [18] to study the fluid mechanics of radial diffusers. The experimental rig was first used to study the effect of inlet conditions on discrete-passage diffuser performance. The pressure recovery of the tested discrete-passage diffuser was found to be primarily dependent on the momentum-averaged inlet flow angle (defined in Section 2.4) and was largely independent of Mach number and

inlet axial distortion [18, 21]. These findings were further assessed and verified by Deniz [11] within a straight-channel diffuser; however, due to the limited access of experimental probes, explanations for the observed diffuser performance trends were largely speculative.

1.4 Objectives of the Current Research

As stated in Section 1.3, it is difficult to experimentally map out the complete flow field in a vaned diffuser, thus making it difficult to establish a causal link between overall performance and detailed fluid dynamic mechanisms. Recent advances have allowed CFD to become both a practical and reliable tool for examining these diffuser flow fields; a computational investigation has therefore been undertaken to provide additional fluid mechanical information to complement previous experimental work performed at MIT, particularly the recent work of Deniz [11].

A CFD solution provides a complete body of flow field information which can be used to explain experimental findings and suggest further complementary physical or numerical experiments. Before utilizing such a computational result, the solution must be validated against any available experimental data to ensure reliability. Once this agreement is established, the code may then be used to describe the flow field in regions not accessed by experimental probes.

To this end the objectives are as follows :

- To computationally examine the flow in the straight-channel diffuser geometry of Deniz [11] subjected to variations in the inlet flow conditions, and to assess the computed performance trends against the experimentally measured result. This serves to establish the physical soundness of the computations.

- To utilize the numerical result to establish the link between the fluid mechanics occurring within the straight-channel diffuser and its performance. Specifically:

    1. To explain the effect of flow angle on straight-channel diffuser performance.

    2. To examine the effect of inlet axial distortion on diffuser performance.

- To use the newly acquired fluid mechanical insight to suggest possible implications on vaned diffuser design.

1.5 Research Contributions

Completion of the research objectives outlined in the previous section has led to the following contributions to the field of radial diffusers:

- A three-dimensional Navier-Stokes solver was found to adequately model the performance of an experimentally investigated straight-channel diffuser.
- The computed result indicated that diffuser channel performance was primarily dependent on flow vector alignment within the channel. Contrary to the conventional view, channel blockage was found to have only a small effect on channel pressure rise.
- The computed result indicated that overall diffuser performance was largely independent of inlet axial distortion. A spanwise work transfer was shown to prevent localized stall from developing as a result of the inlet distortion, thus preserving diffuser pressure recovery.
- These findings were used to suggest methods of improving straight-channel diffuser design.

1.6 Thesis Organization

The thesis is organized as follows. Chapter 2 presents a detailed description of the investigative approach taken, including a description of the geometry under study, the numerical solver, the test outline, and the performance metrics used. Chapter 3 assesses the computational result against the available experimental data. Chapters 4 and 5 examine the effect of various inlet conditions on diffuser performance, comparing the current

computational result with previously held theories. Finally, Chapter 6 presents an overall summary of the thesis, including the contributions, the design implications, and the recommendations for further study.

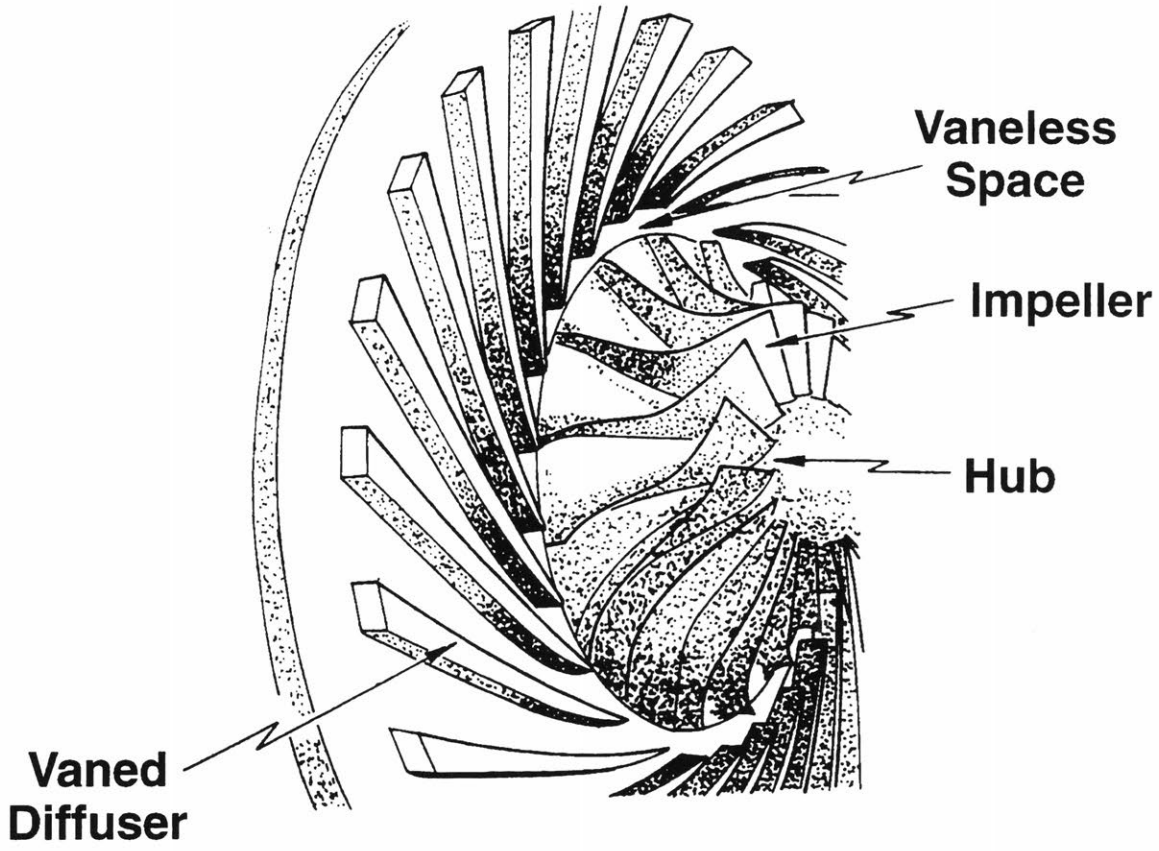

Figure 1-1: A Typical Centrifugal Compressor Stage with Vaned Diffuser; Cumpsty [1989].

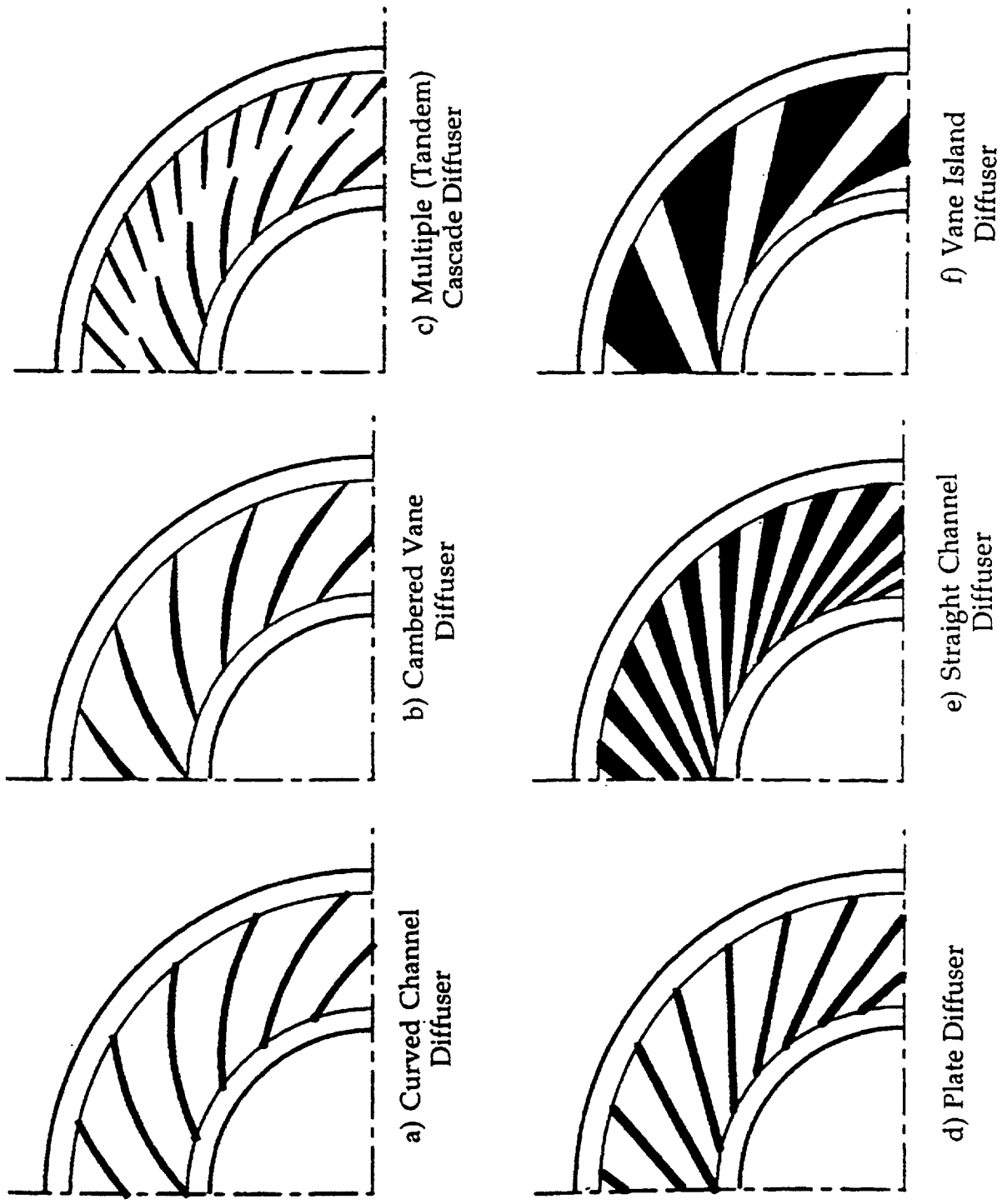

Figure 1-2: Types of Passage Diffusers; Deniz [1996].

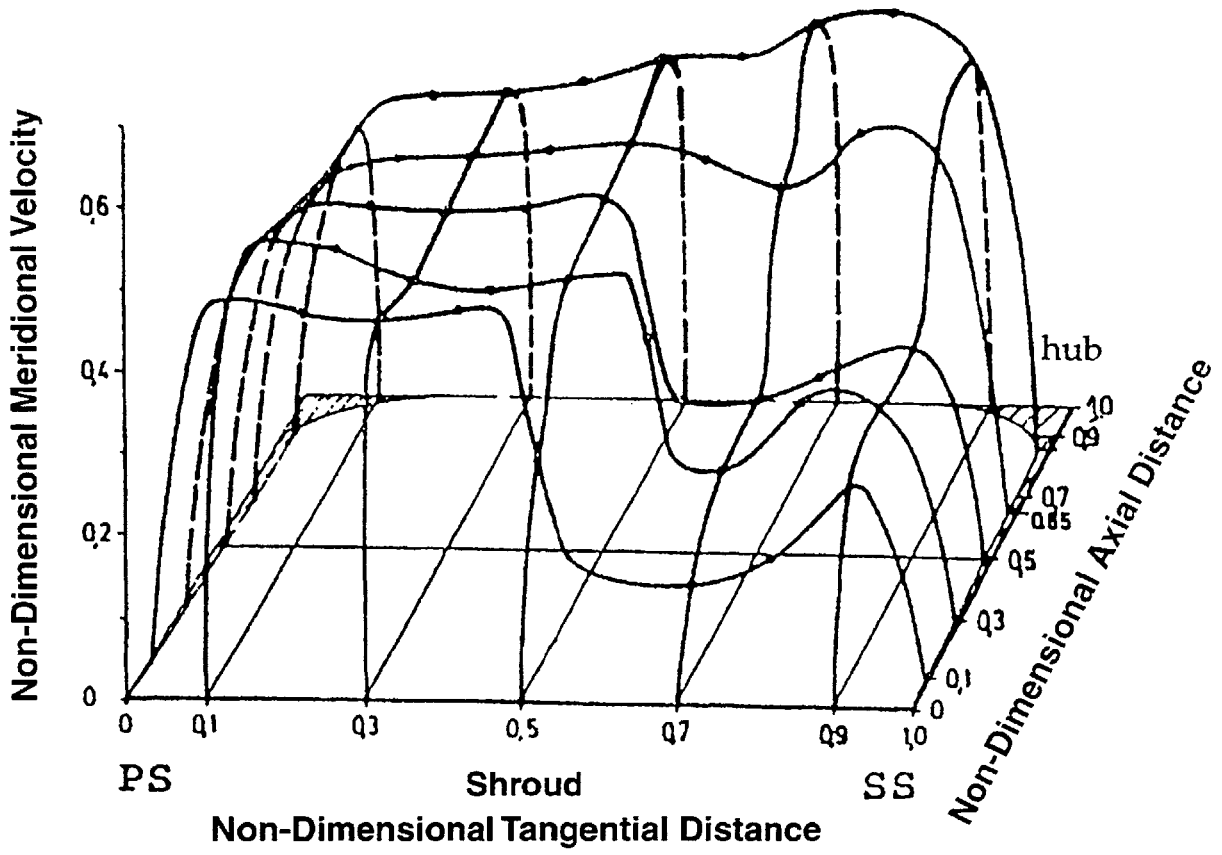

Figure 1-3: A Sample Experimental Velocity Profile at Impeller Exit; data from Eckardt [1977] as reported by Deniz [1996].

Chapter 2

Technical Approach

This chapter outlines the approach used to accomplish the thesis objectives stated in Section 1.4. A description of the diffuser geometry is given, followed by details of the numerical solver. An outline of the computational test cases is then delineated, and finally the parameters which quantify the diffuser flow field are defined.

2.1 Straight-Channel Diffuser Geometry

An experimental straight-channel diffuser was designed by Deniz [11] for assessment against discrete-passage diffusers with similar performance levels. As mentioned in Section 1.2, the straight-channel diffuser is a popular industry design and delivers performance similar to other types of passage diffusers. Therefore, results from investigations of the parameters controlling the performance of such a diffuser would be of interest to the centrifugal compressor community.

The experimentally investigated diffuser geometry is shown in Figure 2-1 and the diffuser geometrical parameters are given in Table 2.1. The diffuser inlet is defined as the leading edge radius, designated Station 1 in Figure 2-1. The semi-vaneless region is located between Station 1 and the throat, designated Station *th* in Figure 2-1. Finally the channel region is located between Station *th* and the diffuser exit radius, designated Station 2 in Figure 2-1. The vane suction side is the vane wall facing toward the inlet

PARAMETER	SYMBOL	STRAIGHT-CHANNEL DIFFUSER
Divergence Angle	2θ	8°
Area Ratio (exit/throat)	AR	2.34
Length-to-Width Ratio	LWR	9.574
Vane Number	N_v	30
Geometric Inlet Angle	α_v	69°
Vane Wedge Angle	β_v	4.0°
Diffuser Inlet Radius	R_1	$0.203m$
Diffuser Exit Radius	R_2	$0.303m$
Diffuser Axial Depth	b	$0.009m$
Throat Area	A_{th}	$0.00013m^2$
Throat Width	W_{th}	$0.014m$
Channel Length	L	$0.138m$
Throat Aspect Ratio (b/W_{th})	AS	0.643

Table 2.1: Parameters for Straight-Channel Diffuser Geometry; Deniz[1996].

radius of the diffuser, while the vane pressure side faces toward the exit radius of the diffuser.

2.2 Numerical Modeling

2.2.1 Computational Geometry

A single passage of this straight-channel diffuser geometry has been modeled computationally using the NEWT grid generator developed by Dawes [6, 8]. The computational mesh, shown in Figure 2-2, consists of $21 \times 61 \times 17$ nodes in the pitchwise, streamwise, and spanwise directions, resulting in 21,080 nodes and 107,328 tetrahedral cells. The computational inlet has been placed at 80% of the leading edge radius, upstream of the leading edge potential field. As a result, a nearly uniform static pressure exists at the computational inlet, which facilitates the imposition of inlet boundary conditions by permitting a circumferentially uniform flow angle profile to be specified. The mesh is symmetric about the midspan in order to provide identical cell connectivities and an identical numerical routine along the hub and shroud walls.

2.2.2 Description of the Numerical Solver

The calculations are carried out using NEWT, a steady, three-dimensional, Navier-Stokes solver developed by Dawes [6, 8]. NEWT has been utilized and verified extensively in a variety of internal flow situations [5, 6, 7]. NEWT uses a structured-based grid of tetrahedra created by its automatic grid generator. The three-dimensional, compressible, Reynolds-averaged, Navier-Stokes equations are discretized in finite volume over the tetrahedra with vertex variable storage. Primary variables are assumed to be piecewise linear across cell faces and fluxes are evaluated to second-order accuracy. Turbulence is modeled using the two $k-\epsilon$ transport equations. Further details of the solver are available in Dawes [6, 8].

2.2.3 Solution Procedure

A calculation using NEWT is set up by specifying stagnation conditions and flow angle at the grid inlet, while pressure is specified at the exit. For all computations, inlet total temperature and exit pressure are specified as uniform. In order to control the velocity profiles entering the diffuser, total pressure and flow angle distributions are specified at the grid inlet. NEWT solves for five output variables at each node, P, ρ, V_r, V_θ, and V_z, which are then used for performance evaluation (see Section 2.4) and post-processing.

2.3 Test Plan, Parametric Study

As stated in Section 1.3.2, the results of Filipenco [18] and Deniz [11] have shown that diffuser performance primarily depends on inlet flow angle, and is largely insensitive to other parameters such as blockage and flow angle skew. These results conflict with other studies [3, 5], and cannot be fully explained due to the lack of detailed measurements, limited by the accessibility of experimental probes in the MIT swirl generator facility. Therefore, the focus of the current computational study (stated in Section 1.4) is to examine the effect of *both* flow angle and inlet axial distortion on vaned diffuser performance, and to utilize the CFD solution to explain the fluid mechanical processes associated with these input

parameters.

To address the effects of these inlet parameters independently, two sets of studies are implemented; these are summarized in Figure 2-3. The *NOMINAL* study is designed to investigate the effect of inlet flow angle over the diffuser operating range, for constant inlet blockage. The *DIST* study is designed to investigate the effect of inlet blockage at different operating points, for constant inlet flow angle. Three operating points are chosen for the *DIST* study: near design ($\hat{\alpha}_1 = 68°$), low mass flow ($\hat{\alpha}_1 = 70°$), and high mass flow ($\hat{\alpha}_1 = 66°$).

In the implementation of the *NOMINAL* study, a uniform inlet total pressure profile is prescribed at the computational inlet while the inlet flow angle is varied. This produces a low and constant level of blockage at the leading edge radius over a wide range of flow angles from 63° to 72° (see Figure 2-3). However, for each *DIST* study, a variety of distorted inlet total pressure profiles are prescribed, while the flow angle is kept nearly constant (inlet flow angle varies by 0.32° for *DIST (68 deg)*). This produces a range of blockage levels at the three different constant inlet flow angles.

Useful and insightful information that can be extracted from these parametric studies will be discussed in detail in Chapters 4 and 5.

2.4 Description of Performance Metrics

In this section, the various figures of merit used to characterize the diffuser performance are defined and discussed. Several previous two-dimensional diffuser studies have used traditional core measurements in order to quantify the inlet flow field [13, 30, 31]. Such methods consider only one data point within the flow field, typically a point near the midspan or within the potential core. On the contrary, many of the parameters in the present study are defined using mass-averaged values of the flow field. It is well documented [11, 18] that such averaging yields a better physical quantification of the flow field than the traditional core measurements. Deniz [11] stresses that detailed traverse measurements and suitable averaging techniques are *required* in order to establish accurate

performance quantification.

All averaged variables are defined as in Deniz [11] for direct comparison with experimental results. Although the computational result allows for such averaging to be performed over two dimensions (the spanwise and circumferential axes), in order to compare with the experimental result of Deniz, the computational data is averaged in one dimension along a traverse of the 17 spanwise nodes along the centerline.

As mentioned in Section 2.2 the output variables of NEWT are P, ρ, and three components of velocity (V_r, V_θ, V_z) at each node. These computed flow variables are used in conjunction with the continuity equation and isentropic relations to obtain the diffuser performance parameters defined below.

Mass Flow

Mass flow is defined by a spanwise integration of product of density and radial velocity along the centerline of the leading edge radius:

$$\dot{m} = 2\pi R_1 \int_0^b \rho_1 V_{r_1} dx \tag{2.1}$$

The mass flow can be obtained from computed values at discrete spanwise points using:

$$\dot{m} = 2\pi R_1 \sum_{i=1}^{16} \left[\frac{\rho(x_i)V_r(x_i) \; + \; \rho(x_{i-1})V_r(x_{i-1})}{2} \right] \cdot (x_i - x_{i-1})$$

Pressure Recovery

Pressure recovery quantifies the performance of the diffuser by relating the overall diffuser static pressure rise to the diffuser inlet dynamic pressure:

$$Cp_{1-2} = \frac{P_2 - P_1}{P_{T_1} - P_1} \tag{2.2}$$

The pressure recovery can also be defined within the semi-vaneless region:

$$Cp_{1-th} = \frac{P_{th} - P_1}{P_{T_1} - P_1} \tag{2.3}$$

and within the channel region:

$$Cp_{th-2} = \frac{P_2 - P_{th}}{P_{T_{th}} - P_{th}} \tag{2.4}$$

Total Pressure

Since the diffuser inlet flow is often nonuniform, Cp can depend on how total pressure is defined, and many different averaging techniques have been utilized to calculate P_T [18]. In order to compare the present computational study with the experimental work of Deniz [11], the availability-averaged total pressure defined by Filipenco [18] is used. This is the static pressure which would result from an isentropic process which decelerates the nonuniform inlet flow to zero velocity. The availability-averaged total pressure across the passage span is then:

$$P_T^{\Psi} = \exp\left(\frac{2\pi R \int_0^b \ln(P_T)\rho V_r dx}{\dot{m}}\right) \tag{2.5}$$

The availability-averaged total pressure may be obtained from computed values at discrete spanwise points using:

$$P_T^{\Psi} = \exp\left(\frac{2\pi R}{\dot{m}} \cdot \sum_{i=1}^{16}\left[\frac{\ln(P_T(x_i))\rho(x_i)V_r(x_i) \; + \; \ln(P_T(x_{i-1}))\rho(x_{i-1})V_r(x_{i-1})}{2}\right] \cdot (x_i - x_{i-1})\right)$$

For incompressible flow, P_T^{Ψ} is equivalent to the mass-averaged total pressure given by:

$$\hat{P}_T = \frac{2\pi R \int_0^b (P_T)\rho V_r dx}{\dot{m}} \tag{2.6}$$

The mass-averaged total pressure may be obtained from computed values at discrete spanwise points using:

$$\hat{P}_T = \frac{2\pi R}{\dot{m}} \cdot \sum_{i=1}^{16}\left[\frac{(P_T(x_i))\rho(x_i)V_r(x_i) \; + \; (P_T(x_{i-1}))\rho(x_{i-1})V_r(x_{i-1})}{2}\right] \cdot (x_i - x_{i-1})$$

For compressible flow P_T^{Ψ} and $\hat{P}_T$ differ by only 1% [11, 18], and both definitions can be used to properly specify Cp.

Flow Angle

In accordance with the work of Deniz, a momentum-averaged flow angle is used to define the inlet flow vector. This flow angle is defined using mass-averaged tangential and radial fluid velocities, $\hat{V_\theta}$ and $\hat{V_r}$. The momentum-averaged flow angle is defined as:

$$\hat{\alpha} = \arctan\left(\frac{\hat{V_\theta}}{\hat{V_r}}\right) \tag{2.7}$$

where the mass-averaged tangential velocity is given by:

$$\hat{V_\theta} = \frac{2\pi R \int_0^b \rho V_r V_\theta dx}{\dot{m}} \tag{2.8}$$

The mass-averaged tangential velocity may be obtained from computed values at discrete spanwise points using:

$$\hat{V_\theta} = \frac{2\pi R}{\dot{m}} \cdot \sum_{i=1}^{16} \left[\frac{\rho(x_i)V_r(x_i)V_\theta(x_i) \; + \; \rho(x_{i-1})V_r(x_{i-1})V_\theta(x_{i-1})}{2} \right] \cdot (x_i - x_{i-1})$$

The mass-averaged radial velocity is given by:

$$\hat{V_r} = \frac{2\pi R \int_0^b \rho V_r V_r dx}{\dot{m}} \tag{2.9}$$

The mass-averaged radial velocity may be obtained from computed values at discrete spanwise points using:

$$\hat{V_r} = \frac{2\pi R}{\dot{m}} \cdot \sum_{i=1}^{16} \left[\frac{\rho(x_i)V_r(x_i)V_r(x_i) \; + \; \rho(x_{i-1})V_r(x_{i-1})V_r(x_{i-1})}{2} \right] \cdot (x_i - x_{i-1})$$

Blockage

In order to characterize the level of flow field distortion, a blockage parameter is used. Blockage quantifies the reduction of available flow area as a result of both the develop-

ment of viscous boundary layers as well as inlet distortion presented to the diffuser by the upstream component (the impeller). A_{eff} is the effective area used by the flow, and is calculated by substituting mass-averaged inlet parameters into the continuity and isentropic relations. A_{geo} is the geometric area seen by the flow.

$$B = 1 - \left(\frac{A_{eff}}{A_{geo}}\right) \tag{2.10}$$

where

$$A_{eff} = \frac{\dot{m}\sqrt{\hat{T}_T}}{\hat{P}_T \hat{M}} \cdot \sqrt{\frac{\Re}{\gamma}} \cdot (1 + \frac{\gamma - 1}{2}\hat{M}^2)^{\frac{\gamma+1}{2(\gamma-1)}} \tag{2.11}$$

and

$$A_{geo} = 2\pi R b \cos\hat{\alpha} \tag{2.12}$$

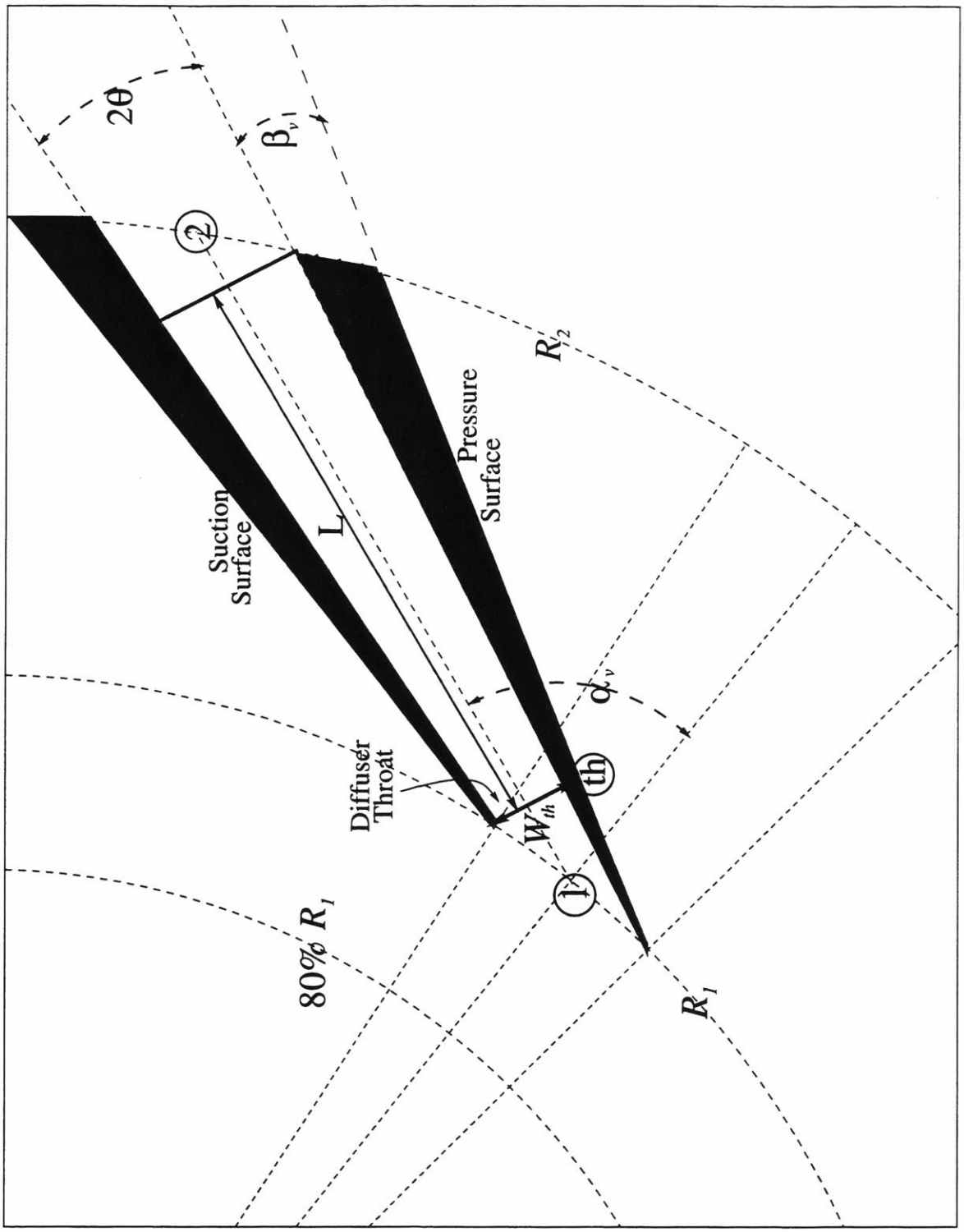

Figure 2-1: Straight-Channel Diffuser Geometry.

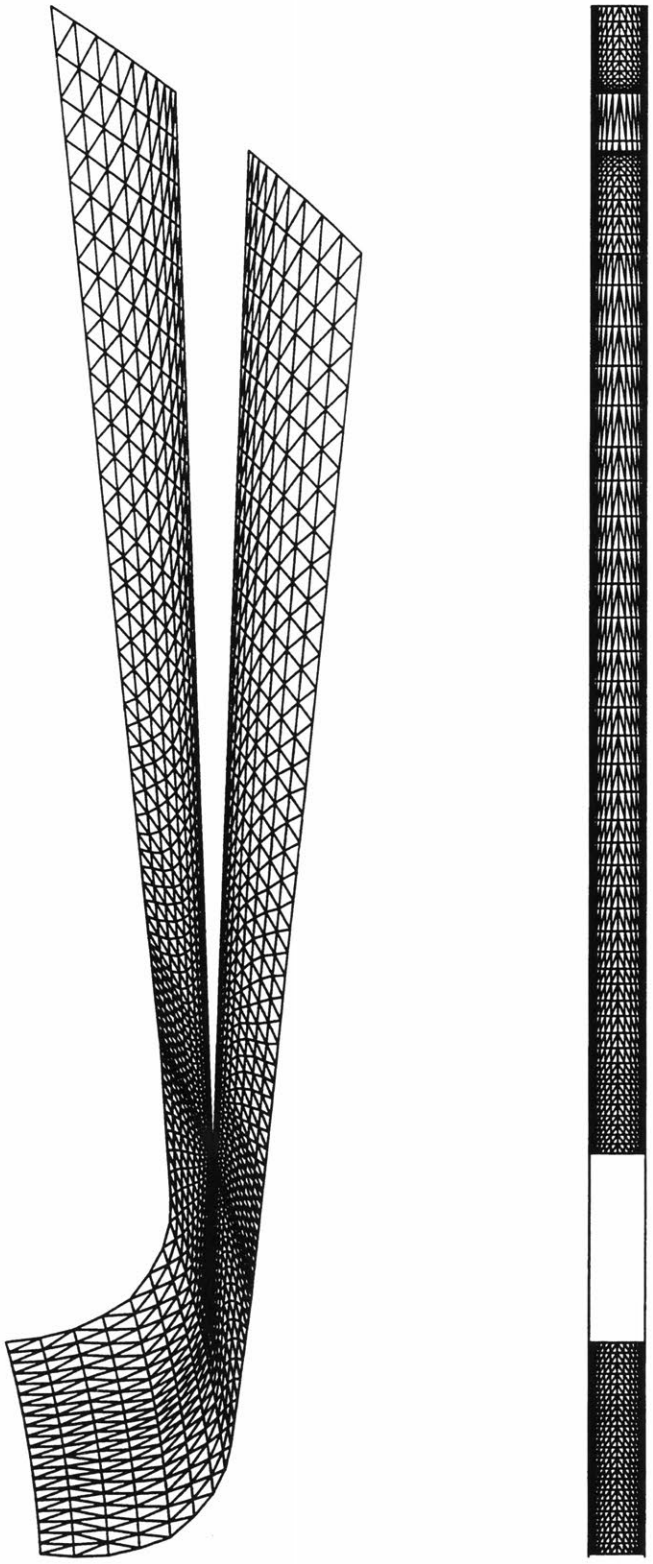

Figure 2-2: Straight-Channel Diffuser Computational Mesh.

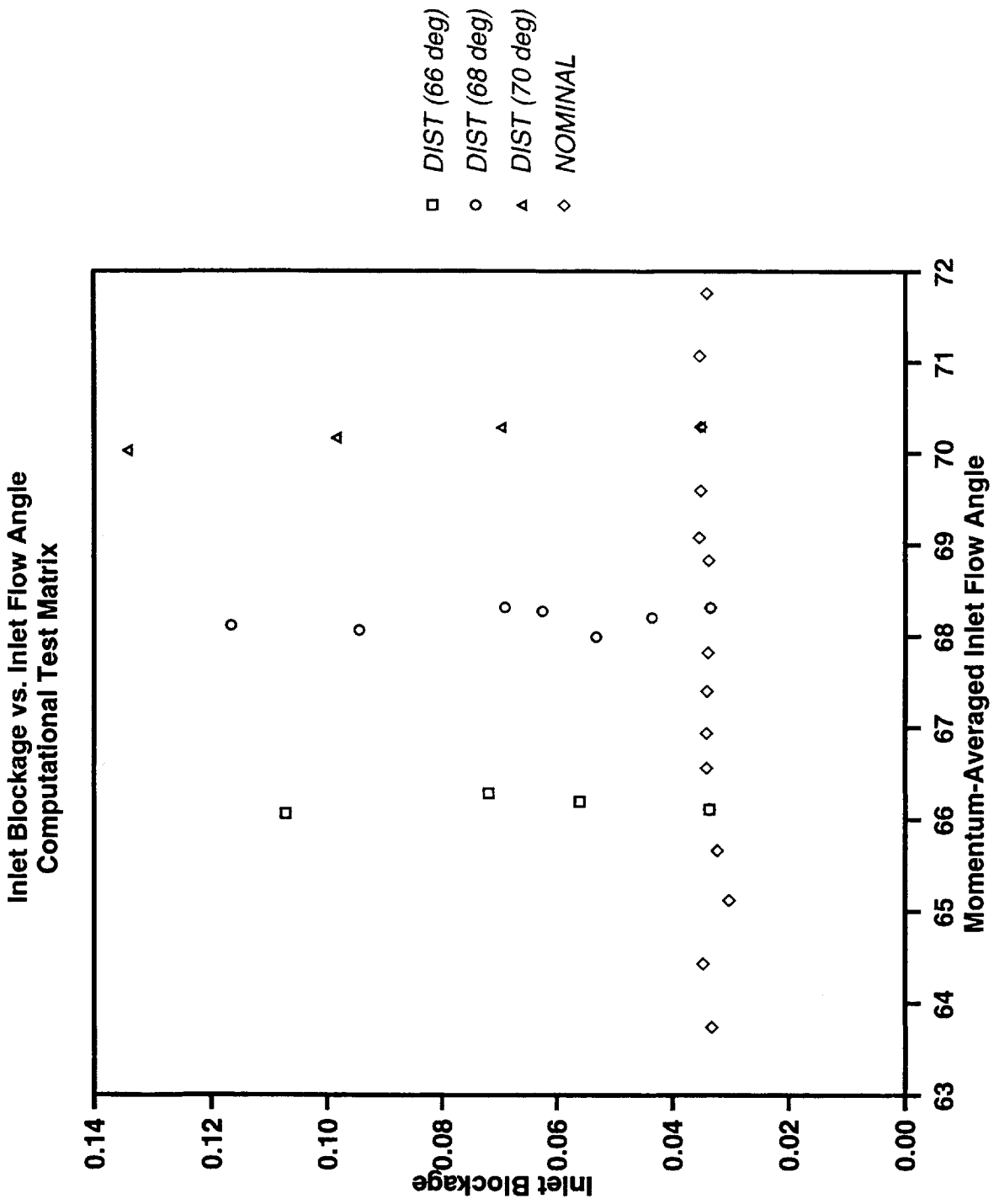

Figure 2-3: Computational Test Matrix; Inlet Blockage and Inlet Flow Angle are Varied Separately for Each Study.

Chapter 3

Assessment of Computational Results Against Experimental Measurements

This chapter assesses the computational results against the experimental data of Deniz [11]. A comparison of inlet conditions is detailed first, followed by an examination of performance data. Finally, these results are used to measure the degree of utility of the NEWT solver for addressing the technical objectives delineated in Section 1.4.

3.1 Inlet Conditions

An important feature of the MIT swirl generator used by Deniz is its ability to create a variety of profiles at the inlet of the test diffuser. Injection and suction slots located in the hub and casing walls upstream of the diffuser inlet are used to control the axial velocity distribution, through the addition and removal of mass flow within the wall boundary layers. The inlet velocity profile of the CFD solution is controlled by adjusting the boundary conditions (the total pressure and flow angle profiles) at the inlet to the computational domain. As a result, the diffuser inlet flow angle distributions can be made similar in both the experiment and the computation.

Figure 3-1 shows the inlet flow angle distribution from hub to shroud for a sample experimental case with no injection/suction control and the inlet profile of a computational result from the undistorted *NOMINAL* study. Figure 3-2 shows the inlet flow angle distribution of an experimental case with a high degree of injection/suction control and the profile of a highly distorted computational result from the *DIST* study. The results of Figure 3-1 and Figure 3-2 show good agreement between the computational and experimental inlet flow angle distributions, and demonstrate that the CFD solution produces comparable levels of inlet flow angle distortion.

Injection/suction boundary layer control also affects the inlet P_T profile, and as a result, the amount of inlet blockage can be adjusted in the experiment. Adjusting the inlet boundary conditions of the CFD solution can create a similar effect. However, because the computational inlet is located far upstream (80% of the leading edge radius) from the true diffuser inlet, any P_T distortion prescribed at the computational inlet is substantially reduced in the vaneless region ahead of the diffuser inlet. This distortion attenuation is thought to be caused by a spanwise work transfer within the region between the computational inlet and the diffuser leading edge radius. As a result, levels of diffuser inlet blockage in the computational result are lower than in the experiment. Figure 3-3 and Figure 3-4 show the inlet P_T distributions for the corresponding experimental and computational cases shown earlier in Figure 3-1 and Figure 3-2. These sample distributions show the lower level of inlet P_T nonuniformity present in the computational cases; the reduced P_T distortion causes lower levels of inlet blockage in the computation, as shown in Table 3.1.

Table 3.1 shows a comparison between experimental and computed values of flow angle, blockage, and Mach number at the leading edge plane of the diffuser vanes. The computed flow variable ranges lie within the range of the experiment, indicating that the computation can adequately model the inlet flow field seen by the experimental diffuser.

FLOW VARIABLE	EXPERIMENT		COMPUTATION	
	min	max	min	max
$\hat{\alpha}_1$	62.79°	70.54°	63.74°	71.76°
B_1	.02	.37	.03	.14
$\hat{M}_1$	.15	1.15	.56	.83

Table 3.1: Comparison of Inlet Flow Field Parameters.

3.2 Diffuser Performance

Once the inlet flow conditions of the computation have been shown to match the experiment, it is important to determine if these similar inlet parameters produce similar output. The only output measured in the experiment is wall static pressure measurements along the diffuser channel centerline from inlet to exit. From this pressure data, Cp at stations along the channel centerline from inlet to exit can be evaluated.

3.2.1 Overall Pressure Recovery

Figure 3-5 displays the computed overall pressure recovery vs. inlet flow angle characteristics against all of the available experimental data, which include both distorted and undistorted inlet profiles. In order to facilitate the comparison, the results in Figure 3-5 are reproduced in two separate graphs with one focusing on the experimental and the other on computational results.

Experimental Result

Figure 3-6 shows overall pressure recovery vs. inlet flow angle from the experimental data, consisting of both undistorted and distorted data. When the availability-averaged pressure recovery, Cp^{Ψ}_{1-2}, and the momentum-averaged inlet flow angle, $\hat{\alpha}_1$, are considered, Cp^{Ψ}_{1-2} depends primarily on $\hat{\alpha}_1$ and appears to be independent of the degree of inlet distortion. In addition, the experimental measurements show a monotonic, nearly-linear increase in Cp^{Ψ}_{1-2} with increasing $\hat{\alpha}_1$, until the initiation of rotating stall at $\hat{\alpha}_1 = 70.3°$.

Computed Result

Figure 3-7 plots the Cp^{Ψ}_{1-2} vs. $\hat{\alpha}_1$ characteristics for all of the computational data, consisting of both the *NOMINAL* and *DIST* studies. Since the computations have been implemented for a single passage of the straight-channel diffuser, multi-passage phenomena such as rotating stall cannot be modeled. Instead, the occurrence of massive flow separation off of the vane suction surface leads to a decrease in Cp^{Ψ}_{1-2} observed for $\hat{\alpha}_1 > 68.3°$; this can be taken as an indication of stalling flow in the computation.

As can be seen in Figure 3-5, for $\hat{\alpha}_1 < 65°$ the trend of the computations do not follow the experimental result. According to Deniz [12], the MIT Swirl Generator and diffuser stage could not achieve momentum-averaged inlet flow angles below 65.9° without the application of a high degree of injection/suction control. In other words, the diffuser in this situation is subjected to a reasonably high degree of axial inlet distortion. It is tentatively argued that the lack of agreement in this flow range is due to a lack of undistorted experimental flow data. For these reasons, assessment against experiment is focused on the flow range between 65.9° and the initiation of rotating stall in the experiment at 70.3°. Within this operating range, agreement between the computed result and experiment is good.

The computed results in the *DIST* study capture the invariance of diffuser performance to inlet distortion in accord with the experimental result. Figure 3-8 plots $\hat{Cp}_{1-2}$ vs. B_1 for each computed *DIST* study. At each operating point ($\hat{\alpha}_1 = 66°$, 68°, and 70°), diffuser performance is weakly dependent on inlet blockage. Figure 3-9 shows similar plots of the experimental data, in which $\hat{Cp}_{1-2}$ vs. B_1 is plotted for two different operating points ($\hat{\alpha}_1 = 68°, 70°$). Figure 3-8 captures the behavior found in the experimental result of Figure 3-9. The ability of the computation to capture this measured trend constitutes an adequate assessment of the CFD solution.

3.2.2 Centerline Pressure Distribution

In addition to focusing on Cp_{1-2}, diffuser performance may be compared by examining the pressure rise distribution along the centerline of the diffuser channel. Figure 3-10 shows

the experimental mass-averaged pressure recovery ($\hat{Cp}$) distribution along the channel centerline from inlet to exit. The four curves show that the pressure rise characteristics of the diffuser change with inlet flow angle, or inlet mass flow. A more detailed description of the effect of inlet flow angle on diffuser performance is given in Chapter 4.

Figure 3-11 provides the $\hat{Cp}$ distribution along the centerline for several operating points of the *NOMINAL* computed study. Increasing inlet flow angle has a similar affect on the $\hat{Cp}$ distribution in both the CFD result and the experiment, as can be seen by comparing Figure 3-11 with Figure 3-10. These results show that, in addition to capturing the overall performance of the experiment, the computation is capable of modeling the pressure distribution throughout the diffuser channel for different operating points.

3.3 Chapter Summary

In this chapter the computed results have been assessed against the experimental data and considerable agreement has been demonstrated. The flow fields at the inlet to the diffuser were examined, and the computation was able to reproduce inlet flows similar to experiment. The performance was analyzed, and the CFD result was found to yield similar performance over the operating range of interest. It is important to note that the computation was able to capture the measured trend found by Filipenco [18] and later by Deniz [11]; Cp^{Ψ}_{1-2} was found to be largely insensitive to inlet distortion and inlet blockage when plotted against $\hat{\alpha}_1$. This phenomenon will be further examined in Chapter 5.

These successful comparisons lend confidence to the CFD solution. Once this reliability is established, the computation may be examined in depth for flow features which have not been investigated experimentally. Flow features computed in a reliable CFD result provide an appropriate model with which to view the experimental flow field as well. Chapters 4 and 5 utilize the computation to explain some of the fluid mechanics which occur in vaned diffusers.

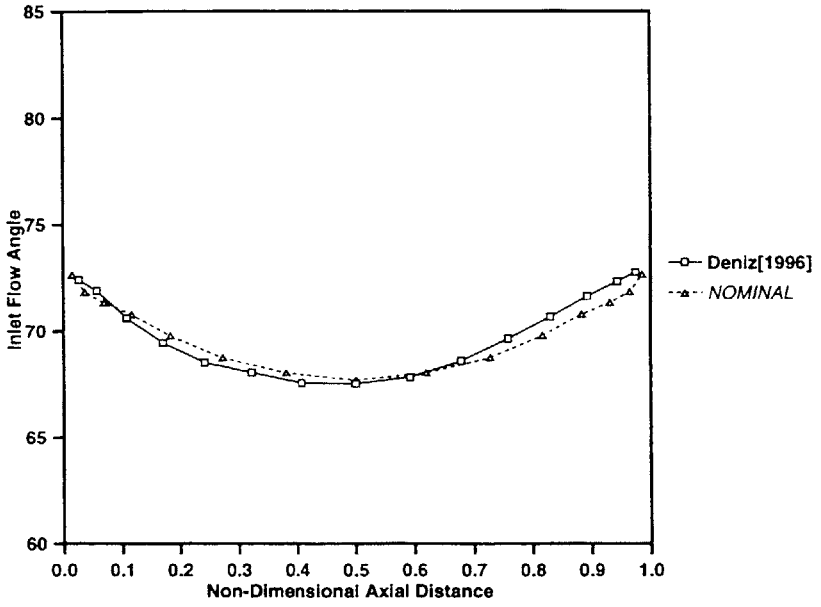

Figure 3-1: Undistorted Inlet Flow Angle Distribution; Computation and Data from Deniz[1996].

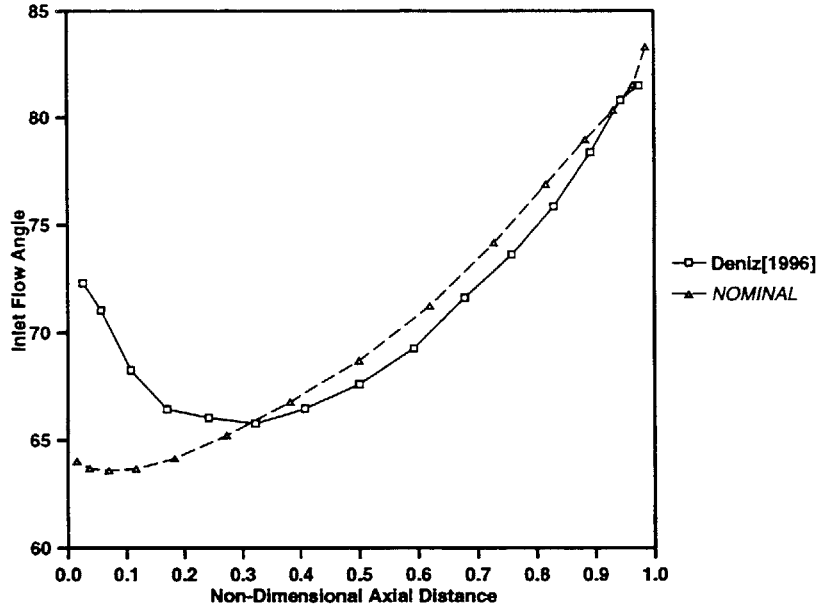

Figure 3-2: Distorted Inlet Flow Angle Distribution; Computation and Data from Deniz[1996].

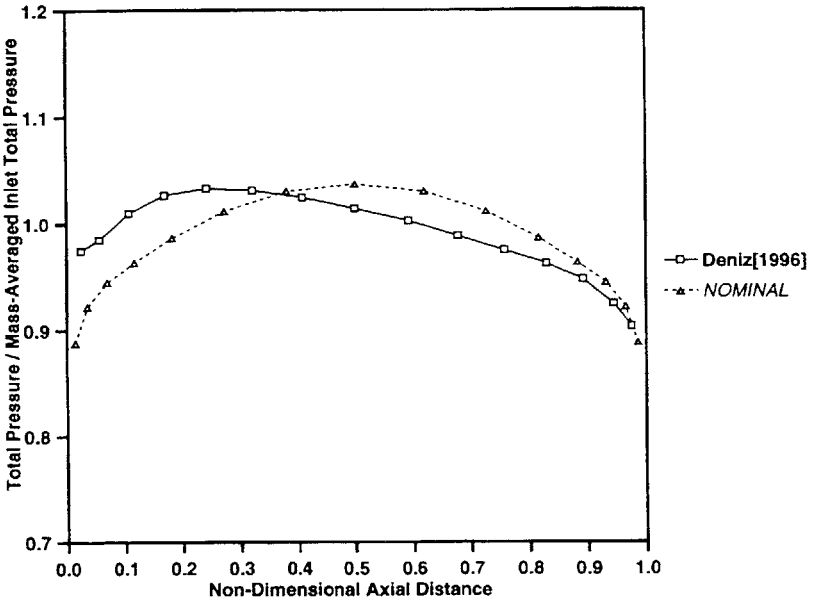

Figure 3-3: Undistorted P_T Distribution; Computation and Data from Deniz[1996].

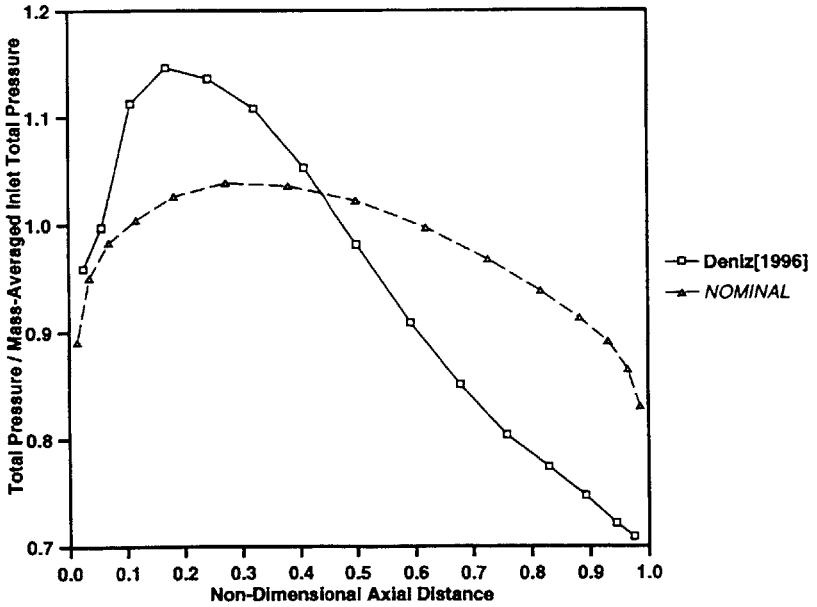

Figure 3-4: Distorted P_T Distribution; Computation and Data from Deniz[1996].

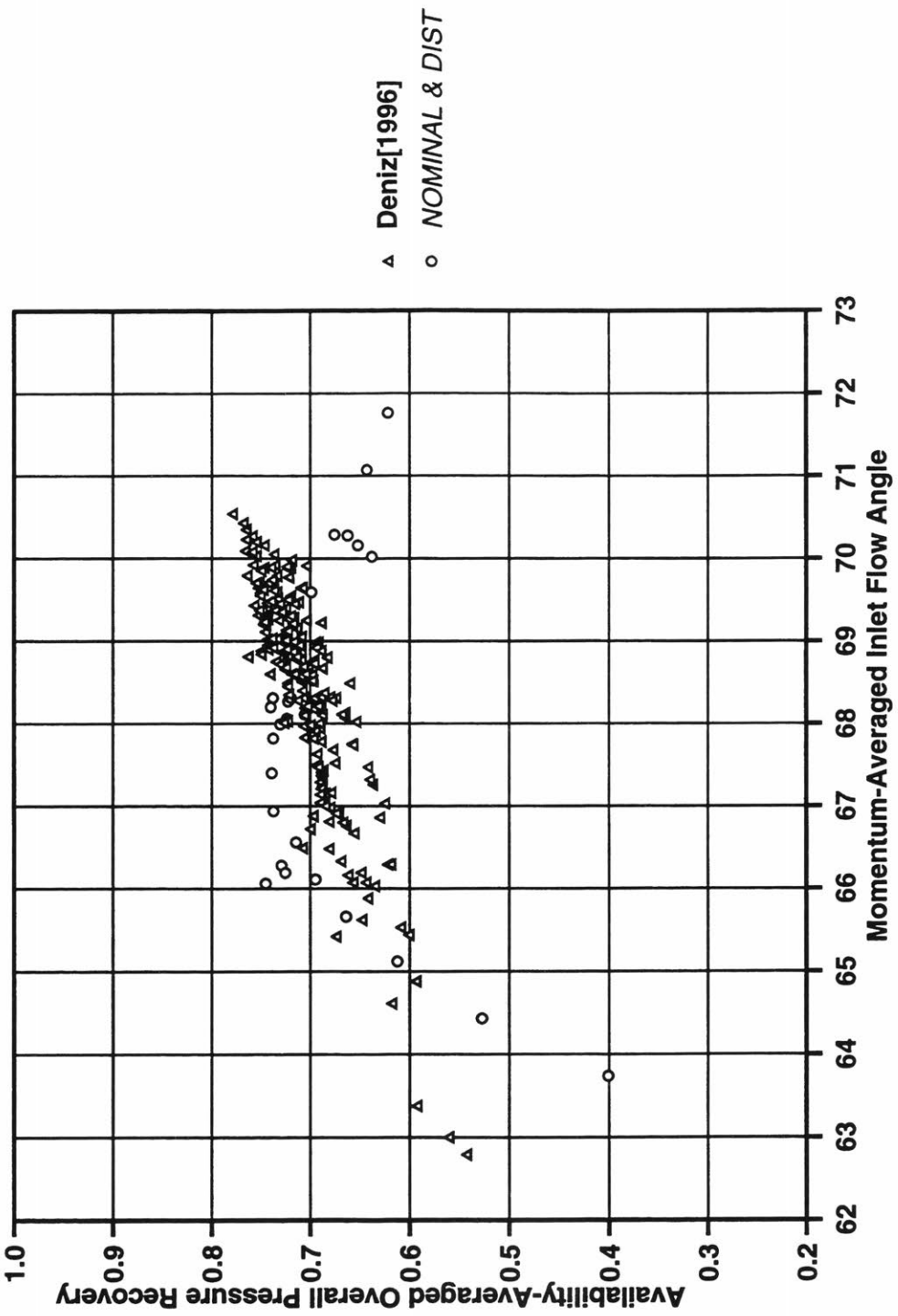

Figure 3-5: Overall Pressure Recovery vs. Inlet Flow Angle; Computation and Data from Deniz[1996].

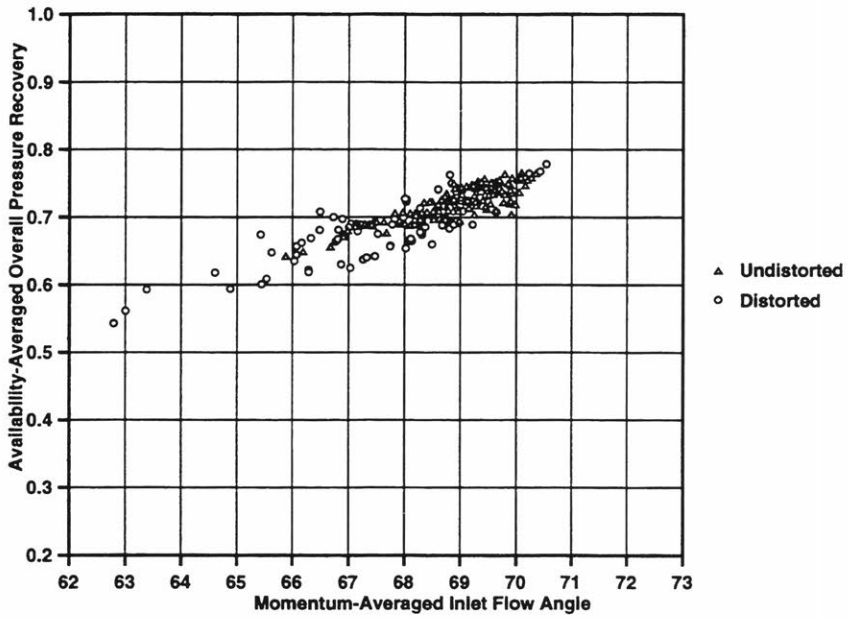

Figure 3-6: Overall Pressure Recovery vs. Inlet Flow Angle; Data from Deniz[1996] Only.

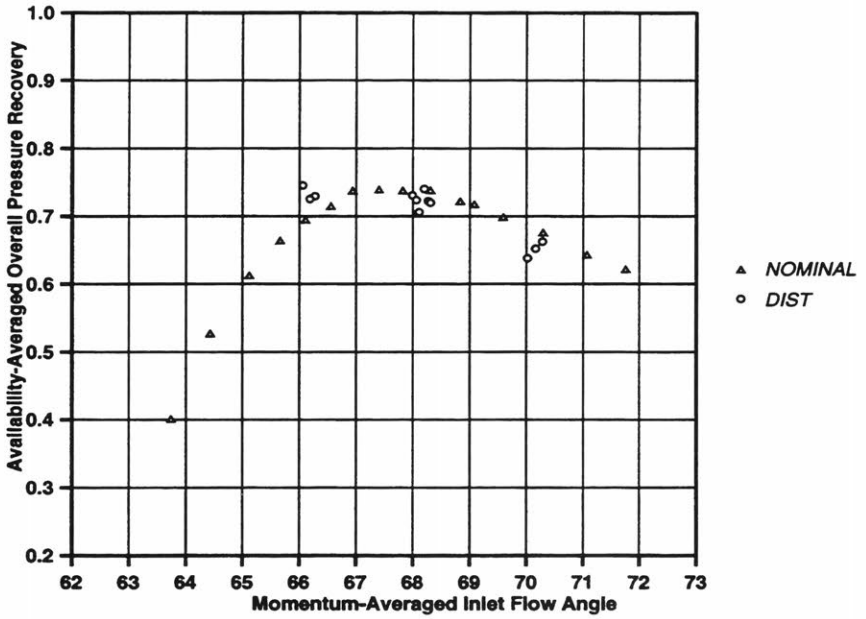

Figure 3-7: Overall Pressure Recovery vs. Inlet Flow Angle; Computation Only.

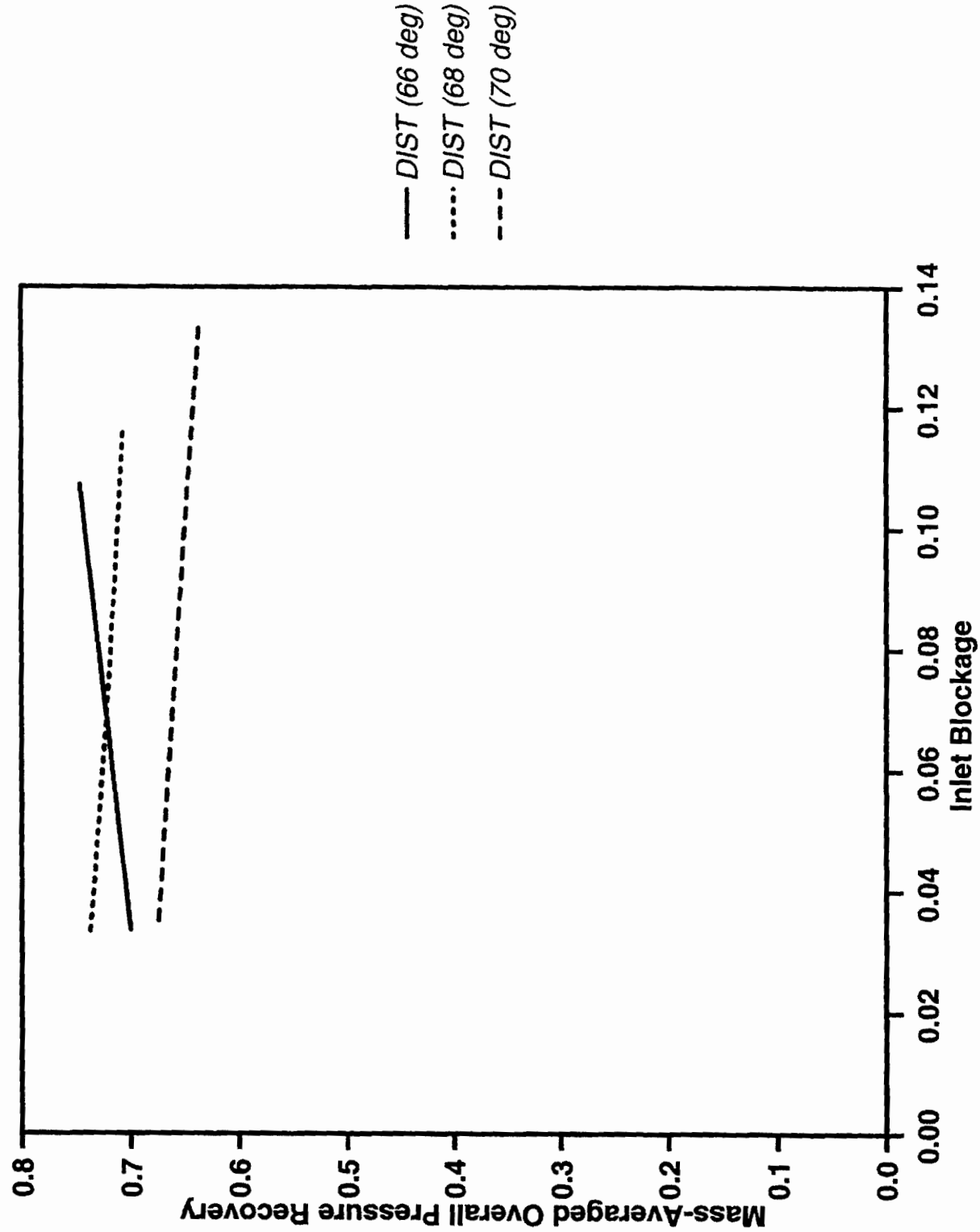

Figure 3-8: Overall Pressure Recovery vs. Inlet Blockage, for Constant Inlet Flow Angles; Computation.

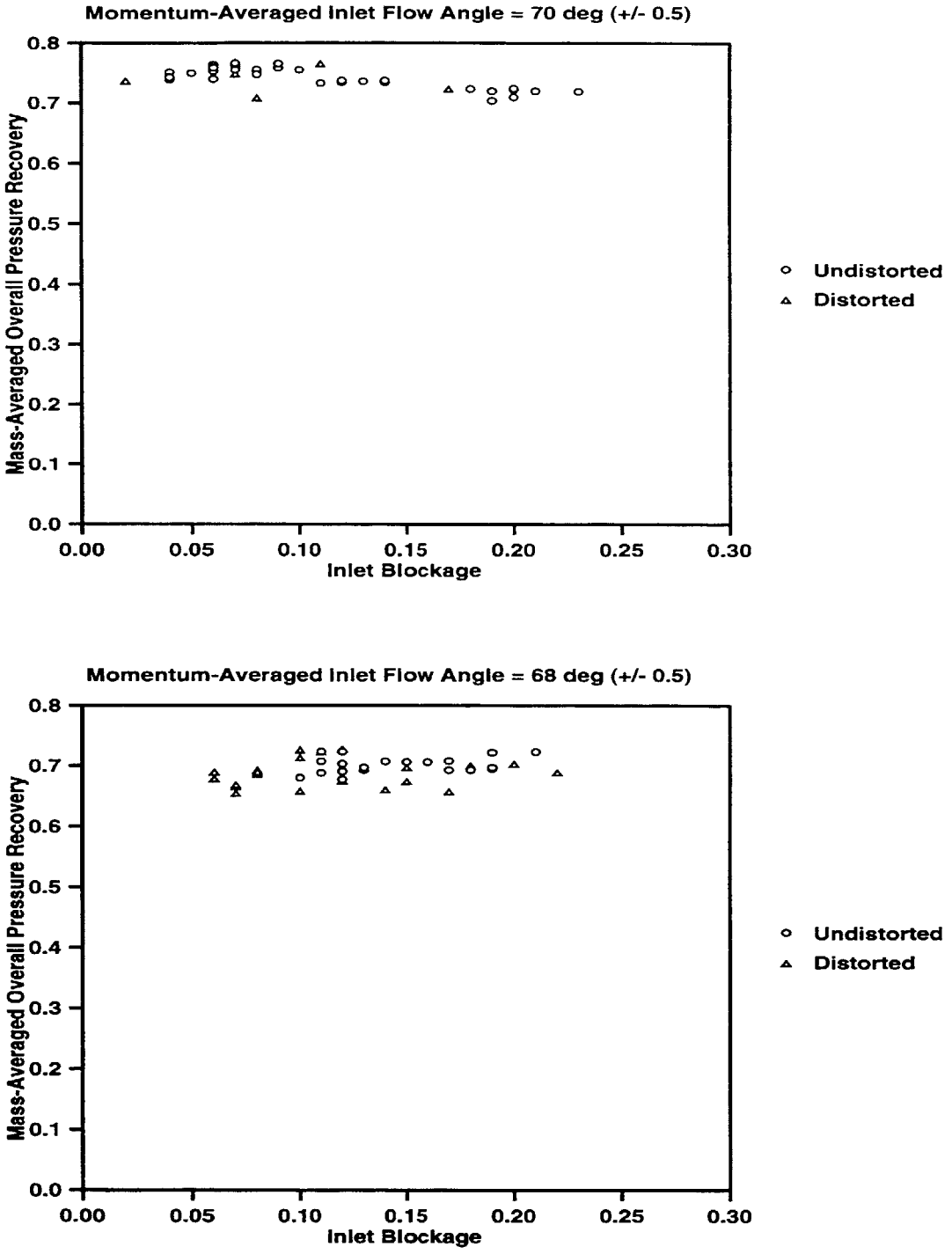

Figure 3-9: Overall Pressure Recovery vs. Inlet Blockage, for Constant Inlet Flow Angles; Data from Deniz[1996].

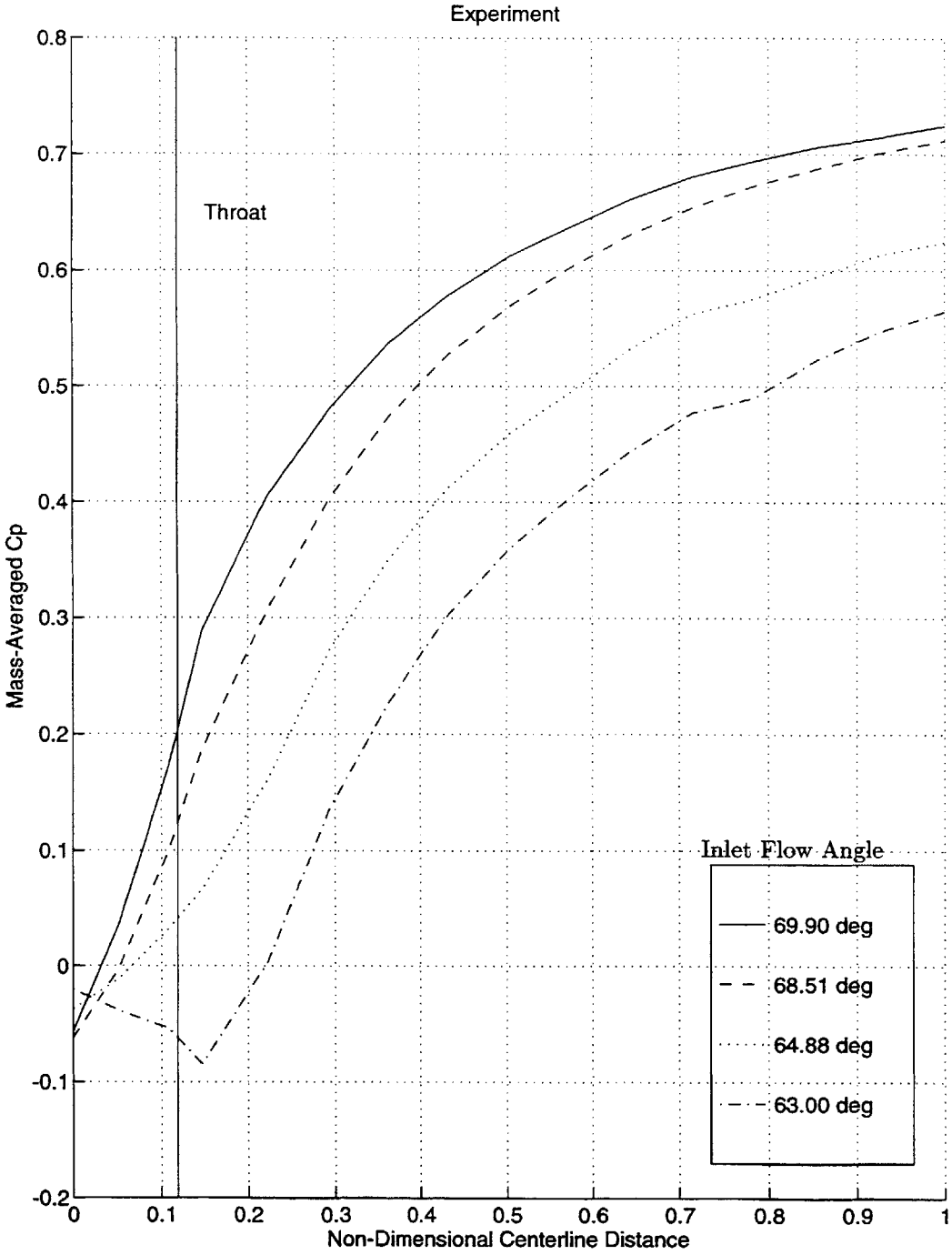

Figure 3-10: $\hat{Cp}$ Distribution Along Diffuser Centerline; Data from Deniz[1996].

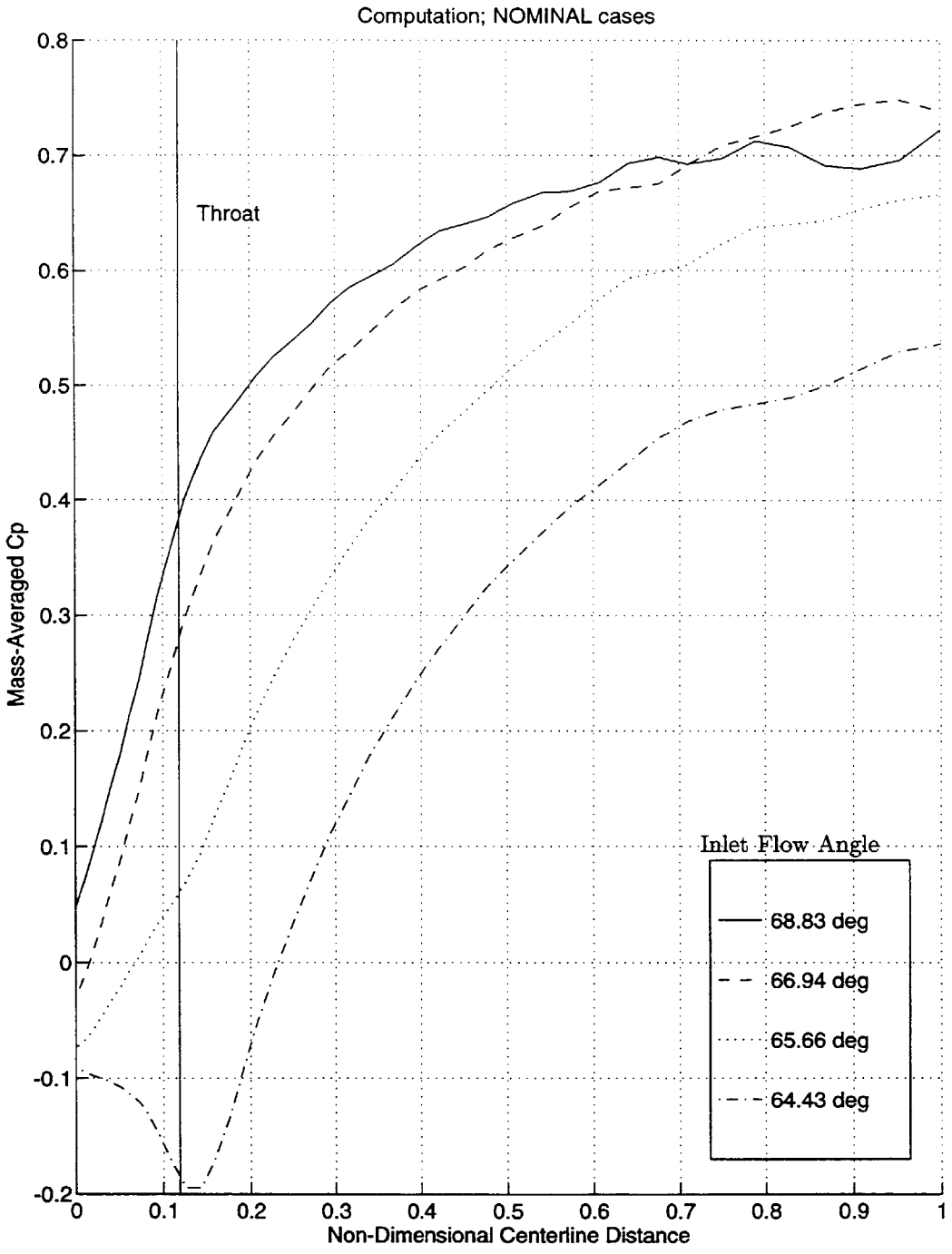

Figure 3-11: $\hat{Cp}$ Distribution Along Diffuser Centerline; *NOMINAL* Study.

Chapter 4

Effect of Flow Angle on Diffuser Performance

This chapter describes the effect of flow angle on straight-channel diffuser performance, as determined through an analysis and synthesis of the computed result. A background of current theories and design methods is given, followed by the numerical results which challenge these ideas. Finally, conclusions and implications of the results are outlined.

4.1 Background

Current theories concerning the effect of inlet flow angle on vaned diffuser performance are outlined in many sources [3, 11, 20]. Inlet flow angle is directly related to mass flow rate, defined in Section 2.4; low flow angles (high $\frac{V_{r1}}{V_1}$) correspond to high flow rates, while high flow angles (low $\frac{V_{r1}}{V_1}$) correspond to low flow rates. Peak pressure recovery occurs at high flow angles prior to the initiation of rotating stall. At low flow angles approaching choke, pressure recovery is substantially reduced [11].

4.1.1 Current Vaned Diffuser Theory

In fluid dynamic terms, it is useful to view the diffuser as a semi-vaneless region followed by a channel region.

Semi-Vaneless Region

Pressure recovery in the semi-vaneless region grows monotonically with increasing inlet flow angle, as shown in Figure 4-1. For a low inlet flow angle, the geometric inlet area (shown as A_{HIGH} in Figure 4-1) is large; the semi-vaneless region acts as a nozzle, accelerating the flow into the throat. For a high inlet flow angle, the geometric inlet area (A_{LOW} in Figure 4-1) is small, and a high level of diffusion occurs between inlet and throat.

Channel Region

As diffusion increases within the semi-vaneless region, the wall boundary layers thicken due to the increasingly adverse pressure gradient. Thickening wall layers in the semi-vaneless region cause higher levels of blockage at the diffuser throat. Extensive studies on two-dimensional conical and rectangular diffusers have shown that increased inlet blockage significantly degrades two-dimensional diffuser pressure recovery [13, 28, 30, 31]. By applying these results to radial vaned diffusers, it has been assumed that as semi-vaneless pressure recovery increases, high boundary layer blockage forces the diffuser channel pressure recovery to decrease. Although overall diffuser pressure recovery rises with increasing flow angle, it has been claimed that Cp_{th-2} must be sacrificed for Cp_{1-th}; good performance *cannot* co-exist in both the semi-vaneless region and the channel [20].

4.1.2 Current Design Practices

The theory discussed in the previous section has been used to develop the current straight-channel diffuser design methodology, which is described in numerous resources [3, 11, 20, 25]. In order to estimate Cp_{1-2}, designers must calculate an approximate value for Cp_{th-2} as follows:

1. The inlet flow conditions and diffuser geometry are used to estimate the semi-vaneless region area ratio, which is used to develop an estimate for Cp_{1-th}.

2. Experimental correlations or boundary layer calculations developed by several researchers [9, 22, 23, 29] are used to estimate the throat blockage. Figure 4-2 shows

such correlations of B_{th} vs. Cp_{1-th}; as stated in Section 4.1.1, increasing Cp_{1-th} is believed to result in increased throat blockage.

3. The large two-dimensional diffuser database can be used to approximate Cp_{th-2}. Figure 4-3 shows a sample of such two-dimensional diffuser data; if the channel geometry (*AR*, *LWR*, and 2θ) and throat blockage are known, the expected Cp_{th-2} can be pinpointed from the diffuser map.

Knowing Cp_{1-th} and Cp_{th-2}, a designer can then develop an estimate for Cp_{1-2}. While this design procedure has seen widespread use, it has also been criticized for relying heavily on correlations, comparisons, and designer experience [4]. A need therefore exists for a rational design procedure based on an understanding of flow processes that underlie the vaned diffuser performance.

4.2 Computed Results & Comparison With Theory

In order to address the need for an improved fluid mechanical description of the vaned diffuser, the computed result is compared with the theory of Section 4.1.1.

4.2.1 Effect of Inlet Flow Angle on Performance Breakdown within a Diffuser

The dependence of Cp_{1-th}, Cp_{th-2}, and Cp_{1-2} on inlet flow angle is first assessed against the theory. Because computed results over the entire flow angle range of interest are required for this comparison, the *NOMINAL* computed result (described in Section 2.3) is used. Figure 4-4 shows the breakdown of Cp_{1-2} into its components, Cp_{1-th} and Cp_{th-2}; each is plotted against the momentum-averaged inlet flow angle. In agreement with theory, the computed result shows that Cp_{1-th} increases monotonically with inlet flow angle, while Cp_{th-2} decreases with inlet flow angle over most of the operating range of interest.

The theory of Section 4.1.1 states that a tradeoff exists between Cp_{1-th} and Cp_{th-2}. This tradeoff is seen in Figure 4-4: over much of the flow range, Cp_{1-th} increases while Cp_{th-2} decreases. In addition, this tradeoff can be illustrated in Figure 4-5, in which the static pressure contours of two *NOMINAL* cases are shown. For $\hat{\alpha}_1 = 65.12°$, minimal pressure rise occurs in the semi-vaneless region, while excellent pressure recovery is observed in the channel. For $\hat{\alpha}_1 = 70.29°$, optimal diffusion occurs in the semi-vaneless region, while the channel performs poorly. Figure 4-5 and Figure 4-4 show that the computed result captures the performance characteristics delineated in the current theory.

4.2.2 Production of Throat Blockage Within the Semi-Vaneless Region

The blockage development of the computed result can also be assessed against theory. A representative boundary layer calculation of B_{th} vs. Cp_{1-th} of Kano et al. [22] taken from Figure 4-2 is plotted in Figure 4-6 along with the entire computed result, comprising of both undistorted and distorted (*NOMINAL* and *DIST*) studies. The computed result agrees well with the calculation of Kano et al.; as semi-vaneless pressure recovery increases, more blockage develops at the throat. However, it must be noted that the distorted computational cases produce the highest levels of throat blockage, while throat blockage in the undistorted cases increases only slightly with increasing Cp_{1-th}. This may indicate that throat blockage depends strongly on the level of inlet blockage present.

4.2.3 Effect of Inlet Flow Angle on Throat Flow Angle

The agreement between the computed result and the theory delineated in Section 4.1.1 ends when the throat flow angle behavior is investigated. Although experimental measurements of throat flow angle are not found in the literature, traditional theory has assumed that the diffuser vanes align the flow so that $\hat{\alpha}_{th}$ is constant and equal to the geometrical centerline angle, regardless of the value of the inlet flow angle, $\hat{\alpha}_1$ [2]. The computed result in Figure 4-7 shows otherwise. As $\hat{\alpha}_1$ increases, $\hat{\alpha}_{th}$ increases as well;

throat flow angle is highly dependent on inlet flow angle in the computation. This result suggests that the channel region of the vaned diffuser must be capable of accommodating a *large* range of flow angles. This is an important concept which has not been considered in current vaned diffuser design practices.

Current diffuser design practices have utilized the body of two-dimensional diffuser data to predict the pressure recovery of the diffuser channel (see Section 4.1.2). However, in these two-dimensional diffuser studies, the inlet flow velocity is aligned with the channel centerline. Therefore it is assumed that both diffuser walls are equally prone to separation. However, in the computed result on the straight-channel diffuser geometry, the large variation in $\hat{\alpha}_{th}$ indicates that, at some operating points, the throat flow velocity is *not* aligned with the geometric channel centerline. This has the implication of possible premature flow separation off of either the suction or pressure side of the diffuser vane.

Figure 4-8 shows the possible difference in inlet flow alignment between traditional two-dimensional diffusers and radial vaned diffuser channels. The $\Delta\alpha$ flow vector deviation present in the vaned diffuser channel due to variation in throat flow angle may cause a premature wall separation which would result in a discrepancy between true two-dimensional diffuser and straight-channel diffuser performance.

4.2.4 Investigation of Channel Pressure Recovery

The computed result of the radial vaned diffuser must now be assessed against two-dimensional diffuser theory and experimental data. Such an assessment serves to determine if performance differences between the two diffuser types exist due to the effect of flow alignment in the vaned diffuser channel. First it is necessary to select the appropriate two-dimensional diffuser dataset for comparison.

Two-Dimensional Diffuser Results

As mentioned in Section 4.1.1, the experimental two-dimensional diffuser data available in the literature has shown that increased inlet blockage significantly degrades diffuser pressure recovery. However, all of these results have used core or midspan measurements in

order to quantify the inlet blockage and inlet P_T. In Section 2.4, such core measurements are said to be inferior to quantification of the flow field by the mass-average of traverse measurements. Although unpublished, Dong [14] has repeated the two-dimensional diffuser studies of Dolan & Runstadler [13] using mass-averaging to quantify the inlet flow field, in contrast to the core measurement technique used by Dolan & Runstadler. Figure 4-9 compares the results of Dong with those of Dolan & Runstadler for similar conical diffuser geometries. Diffuser pressure recovery appears to be much less sensitive to inlet blockage in the result of Dong than in the result of Dolan & Runstadler.

Although in contrast with traditional two-dimensional diffuser theory, the study by Dong emphasizes that if the inlet flow field is properly quantified by a mass-averaging technique, two-dimensional diffuser pressure recovery is only mildly sensitive to inlet blockage. The work of Dong questions both the reliability of two-dimensional diffuser data based on core measurements and the accuracy of the radial vaned diffuser design methods which depend on this data.

Comparison Between a Two-Dimensional Diffuser and a Vaned Diffuser Channel

Among the large two-dimensional diffuser database, the results of Dong best quantify the effect of inlet blockage on two-dimensional diffuser performance. In addition, only the study by Dong utilizes the same mass-averaging method which is used in the computed result. Therefore, it is appropriate to assess the channel performance of the computation against the Dong result.

Figure 4-10 shows $\hat{Cp}_{th-2}$ vs. B_{th} for the computed result compared against the data of Dong from Figure 4-9. The computed result demonstrates a behavior that is in contrast with the traditional vaned diffuser channel theory of Section 4.1.1. The curves of the three *DIST* studies show that channel pressure recovery is weakly dependent on throat blockage, a result that is in agreement with the trend of the Dong result. However, the *NOMINAL* trend is in discord with both the *DIST* studies and the Dong study. If the channel performance of the vaned diffuser were uniquely dependent on throat blockage,

then the entire computed result (both *NOMINAL* and *DIST* cases) would collapse onto one curve. In summary, the following can be inferred from Figure 4-10:

1. Vaned diffuser channel performance must be dependent on some parameter other than throat blockage.

2. The vaned diffuser channel does not perform in a manner similar to that in two-dimensional diffusers.

4.2.5 Effect of Throat Flow Angle on Channel Performance

As stated above, vaned diffuser channel performance must depend on a parameter other than the throat blockage. In Section 4.2.3, throat flow angle is found to vary significantly with operating point ($\hat{\alpha}_1$), and a deviation of $\Delta\alpha_{th}$ is believed to cause premature channel separation. Therefore it is suggested that channel performance may be dependent on throat flow angle.

To verify this hypothesis, Cp_{th-2} vs. $\hat{\alpha}_{th}$ is plotted in Figure 4-11. *The entire computed result of both the* NOMINAL *and* DIST *studies collapses onto a single curve, indicating that, for a given geometry, channel performance is uniquely dependent on throat flow angle, regardless of the diffuser inlet flow profile.* The optimum $\hat{Cp}_{th-2}$ occurs for $\hat{\alpha}_{th} = 63.80°$, which is equivalent to the geometric centerline throat angle of 63.81°. At this throat flow angle, the flow is properly aligned with the channel centerline, and premature channel separation due to flow angle misalignment is not expected. The computed result shows that for *any* type of diffuser inlet flow profile, $\hat{Cp}_{th-2}$ correlates well with $\hat{\alpha}_{th}$. This discovery contrasts sharply with the previous understanding of vaned diffuser channel fluid mechanics, and has wide implications in diffuser design, which will be discussed in Section 4.3.

Additional verification of the hypothesis is made by examining the static pressure contours of Figure 4-5 and the corresponding total pressure contours shown in Figure 4-12:

- **Low Inlet Flow Angle**

  When $\hat{\alpha}_1 = 65.12°$, the throat flow angle is $\hat{\alpha}_{th} = 61.22°$ (see the plot of $\hat{\alpha}_{th}$ vs. $\hat{\alpha}_1$ in Figure 4-7). At this throat flow angle, the flow is nearly aligned with the channel centerline, and premature separation is not expected. In Figure 4-12, the total pressure contours show no evidence of significant flow separation, and the static pressure contours for this case in Figure 4-5 indicate excellent channel performance.

- **High Inlet Flow Angle**

  When $\hat{\alpha}_1 = 70.29°$, the throat flow angle is $\hat{\alpha}_{th} = 69.35°$. At this throat flow angle, flow is severely misaligned with the channel centerline, and separation off of the diffuser vane is expected. The total pressure contours of Figure 4-12 indicate severe flow separation off of the vane suction surface. This is reflected in the poor channel performance as shown by the static pressure contours for this case in Figure 4-5.

The computed results indicate that vaned diffuser channels are more complex than two-dimensional diffusers; the proper alignment of the flow angle with the channel centerline is extremely important to channel performance.

4.3 Conclusions and Implications

4.3.1 Summary of the Computed Result

The main points of the computational result given in Section 4.2 are as follows:

1. Contrary to established view, throat blockage does not strongly affect downstream channel pressure recovery in the straight-channel diffuser. Therefore the increased B_{th} caused by high Cp_{1-th} *does not* result in low Cp_{th-2}. This implies that good Cp_{1-th} can co-exist with good Cp_{th-2}.

2. Poor vaned diffuser channel performance is primarily caused by flow angle misalignment leading to suction surface separation.

These observations are promising because they indicate that good performance in the semi-vaneless and the channel region *can* co-exist.

In order to achieve optimum Cp_{th-2} for a given geometry, the computational result suggests that $\hat{\alpha}_{th}$ must be closely aligned with the geometric centerline throat angle. For the diffuser under investigation (and for many straight-channel diffuser designs), this throat flow angle alignment only occurs for high flow rates, when Cp_{1-th} is far from optimized. Figure 4-4 shows that the optimum Cp_{1-th} and Cp_{th-2} occur at inlet flow angles which differ by nearly 5°. For this reason, the diffuser under investigation achieves reasonable overall pressure recovery over a wide flow range.

4.3.2 Diffuser Design Options

The results presented imply that the designer actually has a choice. A vaned diffuser may be designed to deliver good performance over a fairly wide flow range, or it may be tailored to deliver excellent performance over a reduced operating range. Excellent overall pressure recovery may be achieved by tailoring the geometric centerline throat angle so that in Figure 4-4 the maxima of the Cp_{1-th} and Cp_{th-2} curves lie at the same flow rate. Such a design would also result in a smaller operating range, as Cp_{1-2} would decrease sharply for off-design flow angles. For the investigated diffuser, the curve of Cp_{th-2} may be shifted by designing a concave vane suction surface in the semi-vaneless region in order to increase the geometric channel centerline angle (see Figure 4-13). At first glance, such a design would allow for the simultaneous optimization of Cp_{1-th} and Cp_{th-2} at design point, yielding excellent design Cp_{1-2}.

Unfortunately, a cambered semi-vaneless region may create additional fluid mechanical complications. Typically vaned diffusers are designed with a channel divergence angle (2θ) which lies very close to stall on two-dimensional diffuser performance maps. Concave wall curvature tends to destabilize wall boundary layers; therefore, significant vane camber in the semi-vaneless region may cause early separation along the suction surface. Additionally, using camber to change the geometric centerline throat angle will affect other geometric properties such as exit area and channel length, changing the ideal expected

pressure recovery.

In view of the above, a new design philosophy incorporating the effect of throat flow angle on channel performance needs to be further developed. The main point of this computational study has been to identify the flaws in the current design procedure, and to suggest improvements based on the importance of flow angle to the diffuser performance characteristic.

$$\text{LOW FLOW} \qquad \frac{A}{A_{TH}} = \frac{A_{LOW}}{A_{TH}} < 1 \qquad \text{(DIFFUSING)}$$

$$\text{NOMINAL FLOW} \qquad \frac{A}{A_{TH}} = \frac{A_{NOM}}{A_{TH}} = 1 \qquad \text{(CONST. VEL.)}$$

$$\text{HIGH FLOW} \qquad \frac{A}{A_{TH}} = \frac{A_{HIGH}}{A_{TH}} > 1 \qquad \text{(ACCELERATING)}$$

Figure 4-1: Semi-Vaneless Region Area Ratio Effect; Japikse[1996].

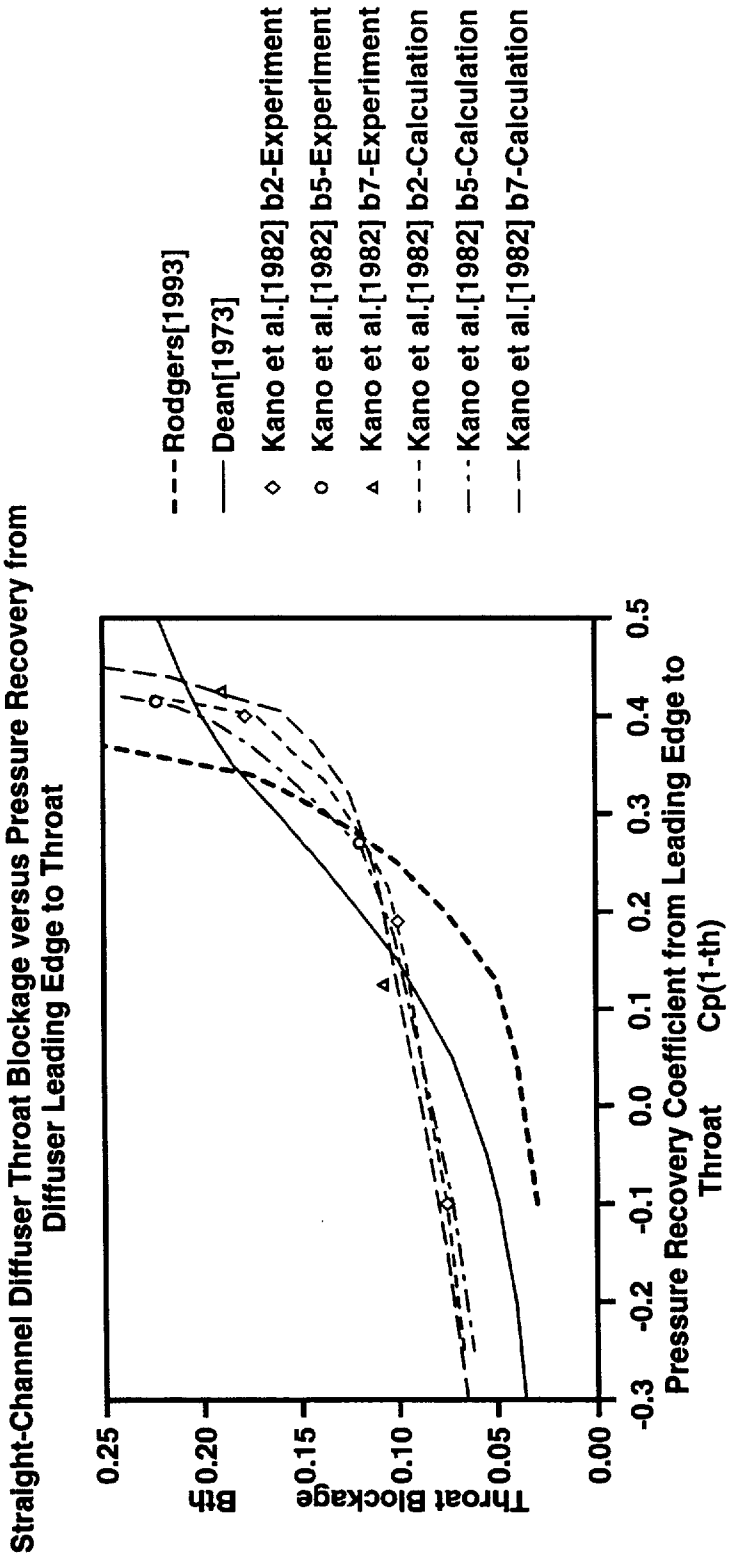

Figure 4-2: Experimental Correlations of B_{th} vs. Cp_{1-th}; Deniz[1996].

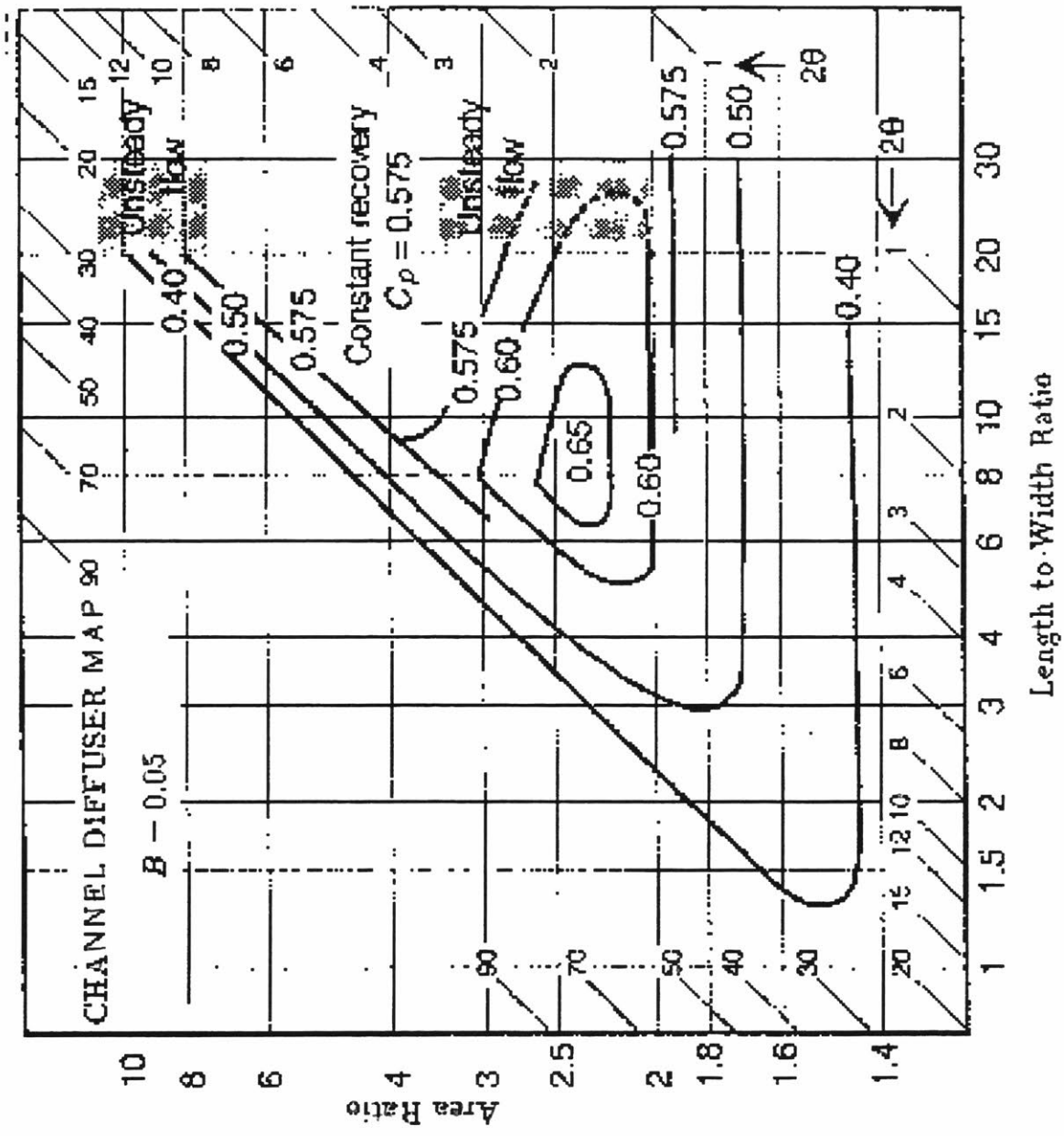

Figure 4-3: Two-Dimensional Diffuser Pressure Recovery Map; Reneau et al.[1967] as reported by Japikse[1996].

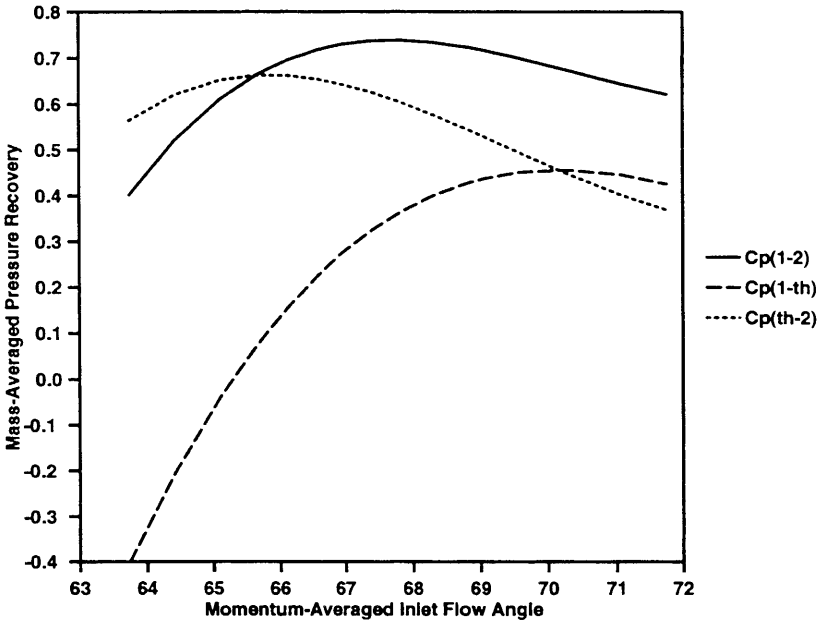

Figure 4-4: Breakdown of Diffuser Pressure Rise; *NOMINAL* Study.

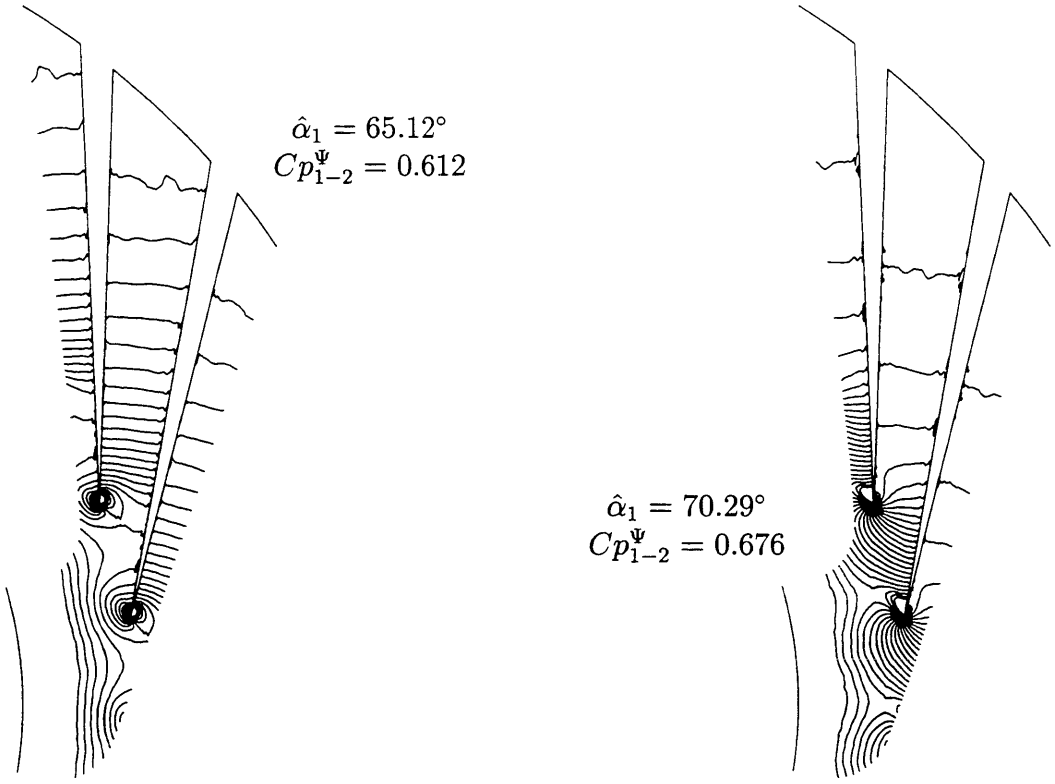

Figure 4-5: Static Pressure Contours for Two Very Different Operating Points; *NOMINAL* Study.

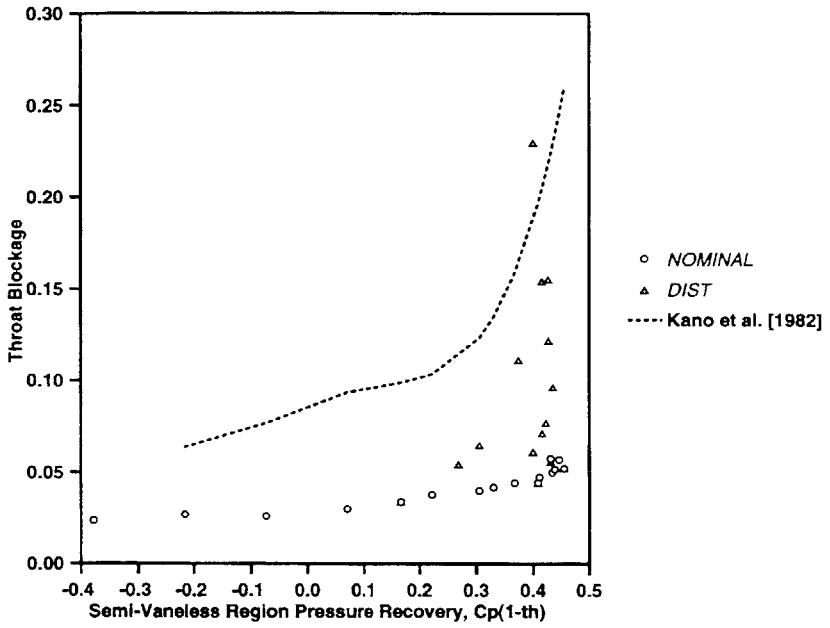

Figure 4-6: B_{th} vs. Cp_{1-th}; Computation and Data from Kano et al.[1982].

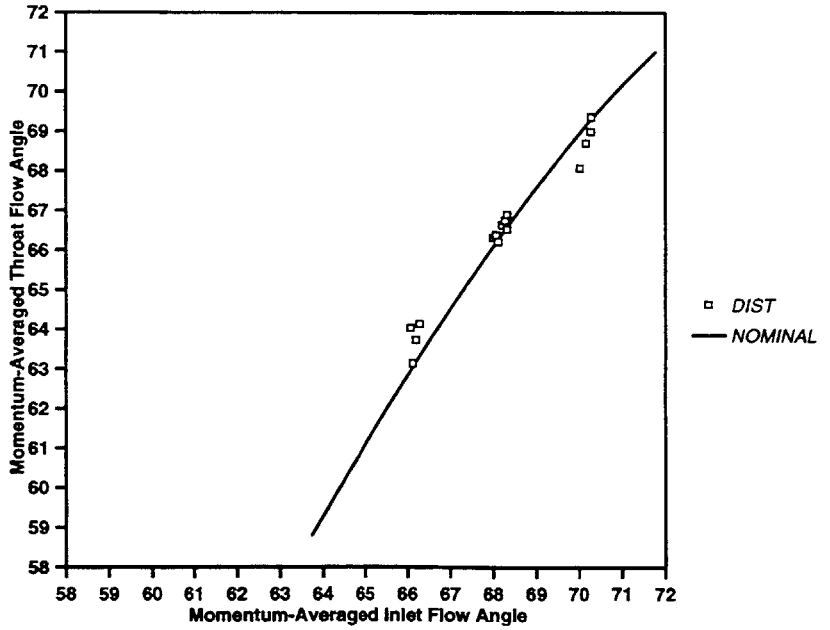

Figure 4-7: Throat Flow Angle vs. Inlet Flow Angle; Computation.

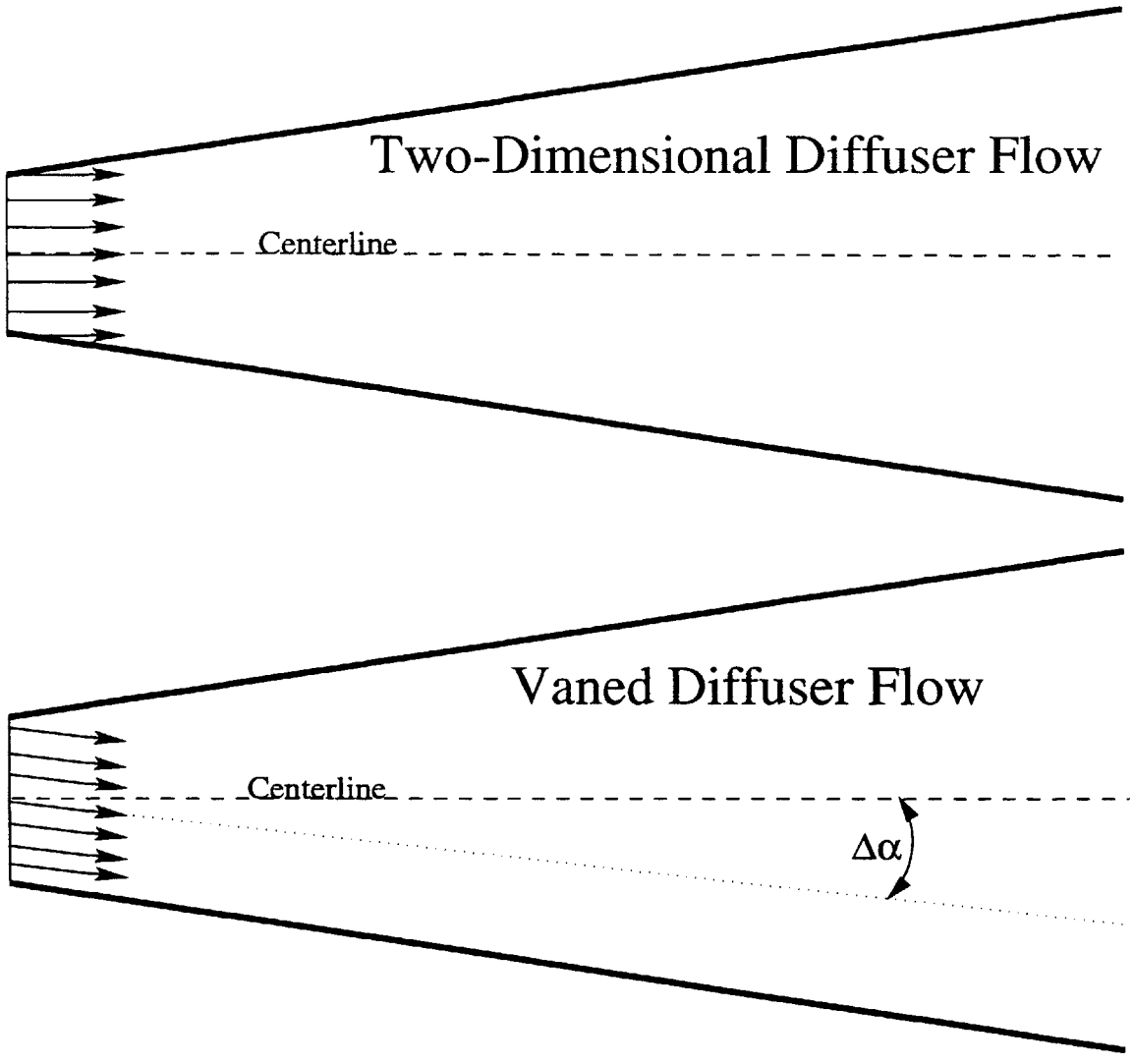

Figure 4-8: Inlet Flow Vector Alignment in Two-Dimensional and Straight-Channel Diffusers.

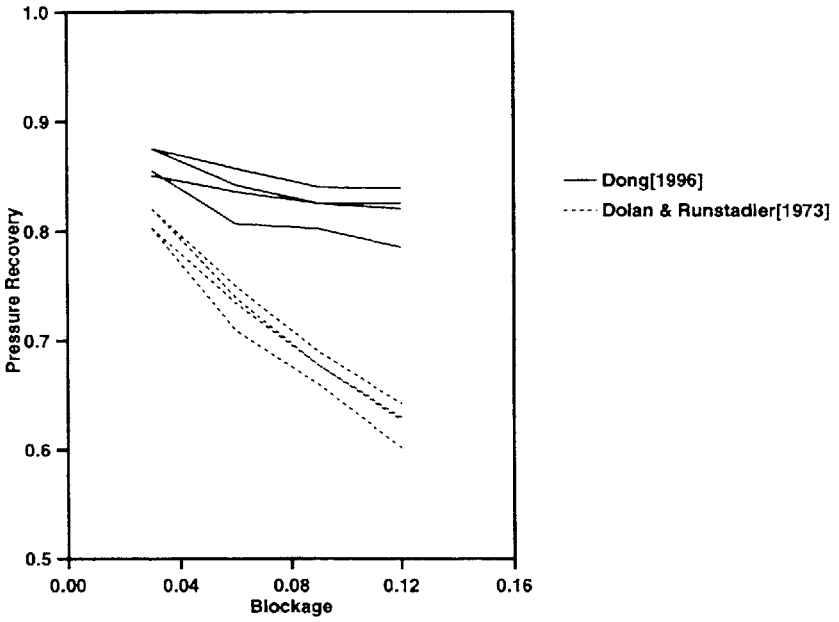

Figure 4-9: Cp vs. B; Two-Dimensional Data from Dong[1996] and Dolan & Runstadler[1973].

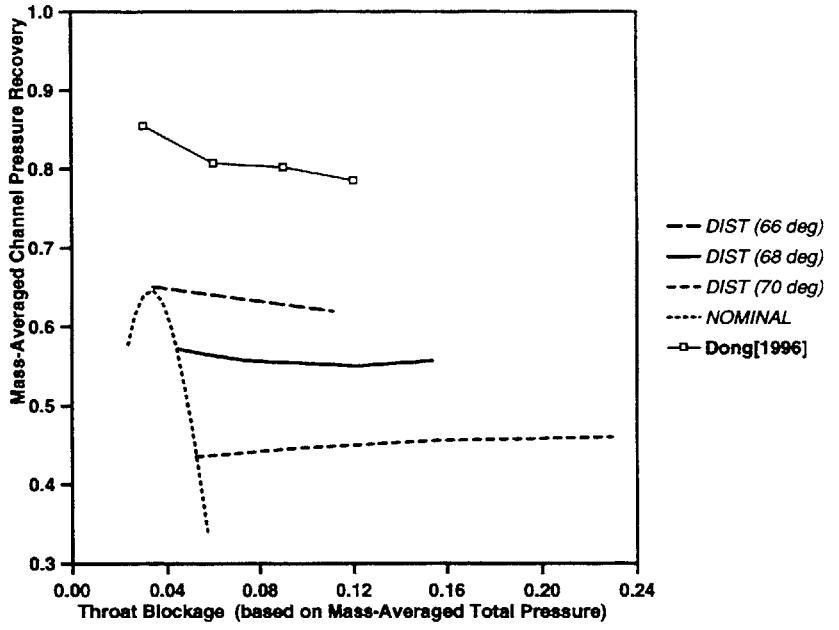

Figure 4-10: Cp_{th-2} vs. B_{th}; Computation and Data from Dong[1996].

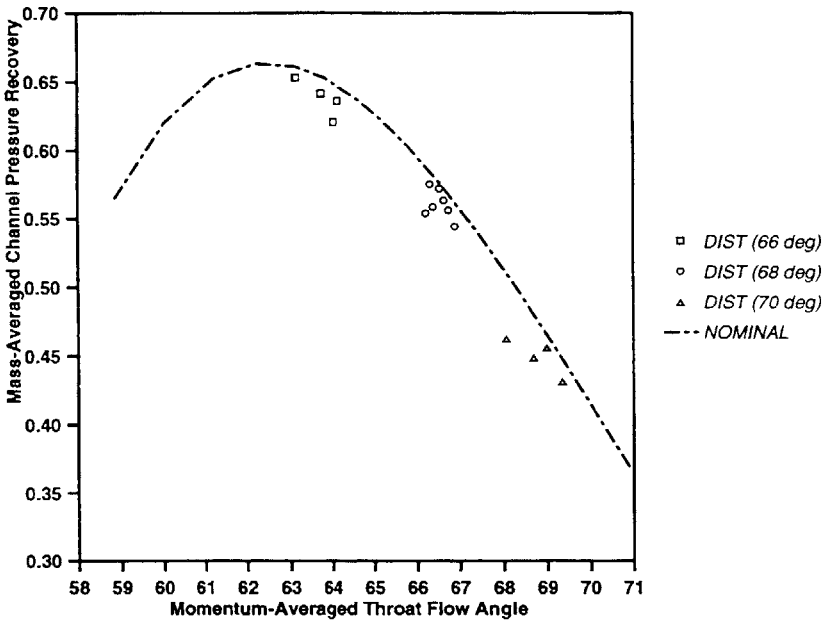

Figure 4-11: Cp_{th-2} vs. $\hat{\alpha}_{th}$; Computation.

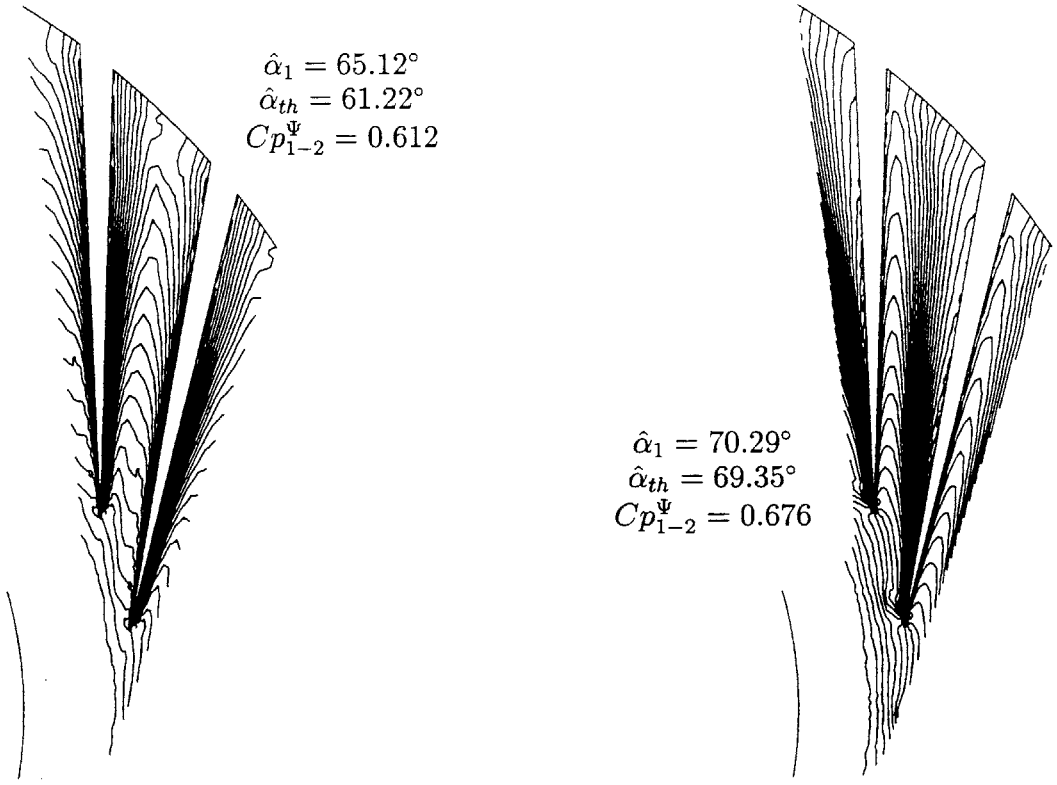

Figure 4-12: Total Pressure Contours for Two Very Different Operating Points; *NOMINAL* Study.

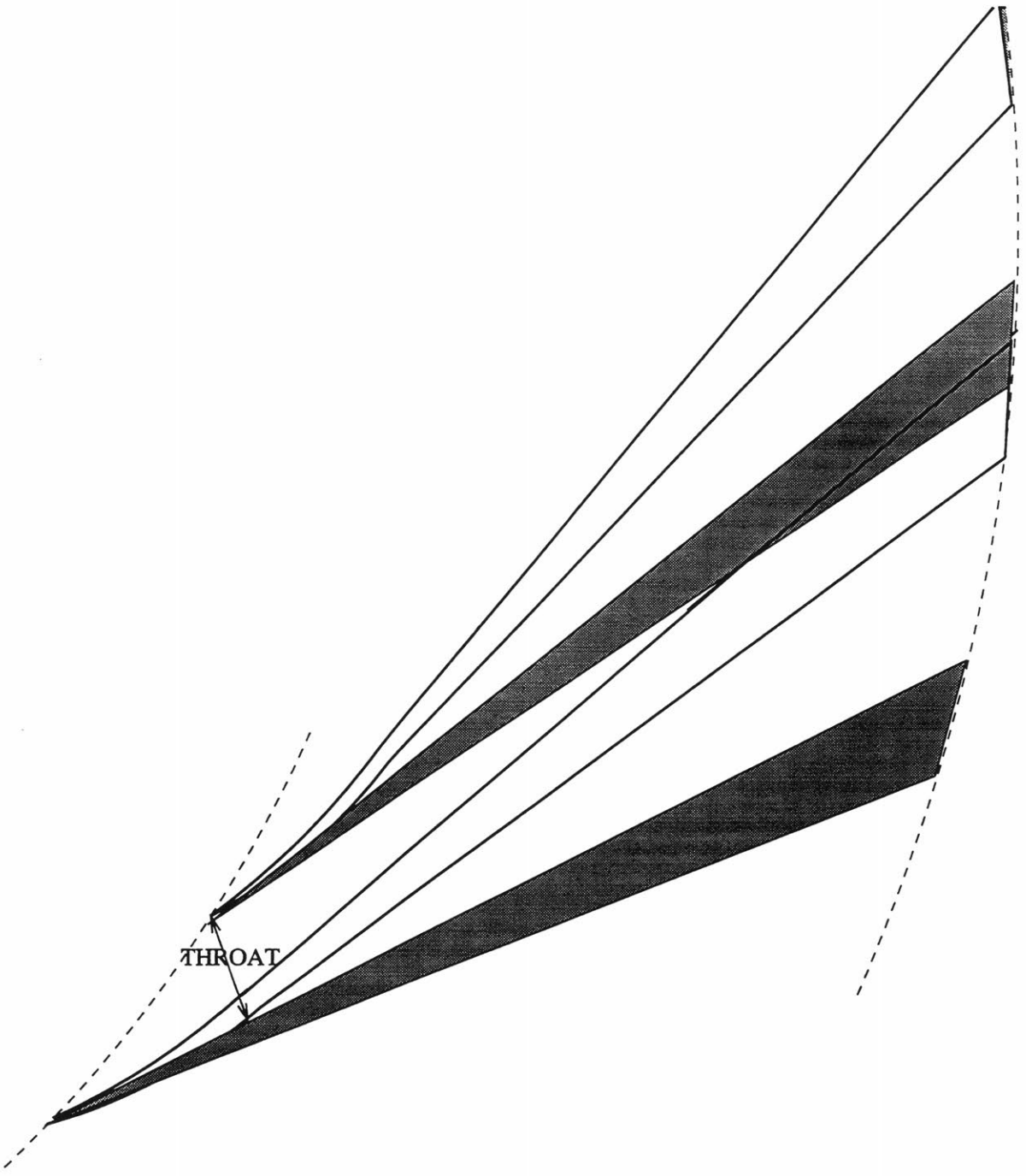

Figure 4-13: Original Straight-Channel Diffuser (Shaded) and Proposed Design with Cambered Semi-Vaneless Region.

Chapter 5

Effect of Inlet Distortion on Diffuser Performance

This chapter describes the effect of inlet distortion on straight-channel diffuser performance. A background of previously held theories is given, followed by observations derived from the computed result. Finally, conclusions and implications of the results are described.

5.1 Background

5.1.1 Previous Experimental Results

Previous research efforts have encountered conflicting results concerning the effect of inlet distortion on diffuser performance. Numerous works [13, 28, 30, 31] have found that the pressure recovery of two-dimensional diffusing passages is significantly reduced by inlet blockage. However, these studies utilized traditional core measurements, which have been found to be an insufficient method of quantifying the inlet flow field (see Section 4.2.4). Although these studies are available in the open literature, their reliability is questionable, and they will not be considered for comparison with the computed result.

Other researchers have used mass-averaging to quantify the inlet flow field. Yoshinaga

et al. [34] studied the effect of axial inlet distortion on radial vaneless diffuser performance, and found that because the distortion remained unmixed at the diffuser exit, overall Cp decreased with increased inlet blockage. Yoshinaga et al. later inserted half-span vanes into the diffuser, which mixed out the nonuniformity and yielded improved pressure recovery. Dutton et al. [15] described the spanwise velocity distribution developed within a radial vaned diffuser rig. Dutton et al. showed that inlet distortion was only partially reduced within the semi-vaneless region, but the flow was fully mixed out at the exit of the diffuser. The benefit of vanes was later supported by Filipenco [18] and Deniz [11], whose measurements showed that overall Cp was not very dependent on inlet axial distortion in both radial discrete-passage diffusers and straight-channel diffusers.

5.1.2 Current Theory

In addition to the experimental results showing the behavior of inlet blockage within diffusers, several theories have been developed to explain how the radial passage diffuser accepts inlet distortion. Filipenco [18] used a control volume mixer-diffuser model to show that for certain diffuser area ratios, the pressure rise is largely insensitive to inlet blockage, provided that flow nonuniformity is mixed out before the diffuser exit. Filipenco theorized that the semi-vaneless space of the discrete-passage diffuser is a strong mixing region; therefore, the behavior of the diffuser could be modeled reliably using the simple control volume model. Utilizing static pressure taps on the casing of the semi-vaneless region, Filipenco was able to show that pressure loading (an indicator of streamwise vorticity) across the leading edge cusps increased with increased inlet distortion. Filipenco argued that streamwise vorticity shed off of the leading edge cusps of the tested discrete-passage diffuser enhanced mixing within the semi-vaneless region. Filipenco theorized that this rapid mixing region created a nearly uniform profile entering the diffuser channel (at the diffuser throat), regardless of the level of inlet distortion.

Dalbert et al. [4] provided support for the theory of Filipenco by using a three-dimensional viscous Navier-Stokes solver to examine flow within a vaned diffuser. Dalbert et al. noticed strong nonuniform flow angle distributions near the diffuser inlet radius, and

resorted to a theory of Traupel [33] to explain why poor performance and separation did not result from such a large inlet flow angle nonuniformity. Traupel recognized that an inlet shear flow (or inlet flow angle nonuniformity) coupled with the presence of the diffuser blades creates a secondary flow field. This secondary flow field sets up vortices which are capable of energizing flow near the blade surfaces, thereby delaying separation. Dalbert et al. were able to observe this secondary flow using particle tracing in the computational result.

5.2 Computational Results

It has been shown in Section 3.2 that the CFD result of the present study is able to simulate the experimental result of Deniz [11]; overall straight-channel diffuser performance is largely insensitive to inlet blockage. The computed result can now be further examined for fluid behavior which will provide an appropriate model of the experimental flow field. In this manner, the CFD result may yield an explanation for the observed insensitivity of diffuser performance to inlet distortion.

5.2.1 Downstream Development of the Inlet Flow Field

The first step in examining the computed result is to determine if the inlet axial distortion is mixed out in the vaned diffuser, as theorized by Filipenco [18] and observed by Yoshinaga et al. [34] and Dutton et al. [15] (see Section 5.1).

The behavior of inlet axial distortion within the vaned diffuser can be investigated by examining different computed results at a single operating point, thereby eliminating any inlet flow angle dependence. The design operating point is selected, and a case from the *NOMINAL* study (low inlet distortion) with $\hat{\alpha}_1 = 68.31°$ is assessed against a case from the *DIST* study (high inlet distortion) with $\hat{\alpha}_1 = 68.11°$. The inlet conditions and performance of these two cases are shown in Table 5.1. Despite the vastly different levels of inlet blockage, the two cases show similar pressure recovery performance.

CASE	$\hat{\alpha}_1$	B_1	$\overline{Cp}^{\Psi}_{1-2}$
NOMINAL, Low Distortion	68.31°	0.033	0.738
DIST, High Distortion	68.11°	0.117	0.706

Table 5.1: Comparison of Low & High Inlet Distortion Cases Near Design Point ($\hat{\alpha}_1 = 68°$).

NOMINAL Case, Low Distortion

This section describes the behavior of the case with a low level of inlet axial distortion ($B_1 = 0.033$). Figure 5-1 shows the flow angle distribution across the span of the diffuser, at different locations along the centerline. The level of flow angle nonuniformity at the inlet is low, and remains quite constant through the diffuser throat. Beyond the diffuser throat (17.5% to 57.5% of the diffuser centerline distance), the flow angle profile becomes more uniform.

Similar behavior can be observed in Figure 5-2, which shows the spanwise total pressure distribution at different locations along the diffuser centerline. The level of P_T nonuniformity remains unchanged from the inlet to the throat of the diffuser. Downstream of the throat, P_T becomes more uniform across the span; P_T increases in the boundary layer near the casing, and decreases near the passage midspan.

DIST Case, High Distortion

This section describes the behavior of the case with a high level of inlet axial distortion ($B_1 = 0.117$). Figure 5-3 shows the spanwise flow angle distribution at different locations along the diffuser centerline. The level of flow angle nonuniformity is very high at the inlet, and, as in the case of low distortion, remains quite constant through the diffuser throat. Between the throat and 17.5% of the centerline distance, the flow angle distribution becomes significantly more uniform. At 57.5% of the centerline distance, α is nearly constant across the span.

By comparing Figure 5-3 with Figure 5-1, one can see the large difference in inlet flow angle distortion between the two cases under study. Further downstream in the diffuser,

this difference is reduced; by 57.5% of the diffuser centerline, the α distributions in each case are both nearly uniform. This comparison illustrates that significant mixing of the distorted inflow has occurred in the diffuser. It is noted that in both cases under study, the flow angle distributions remain largely unchanged upstream of the diffuser throat.

Figure 5-4 shows the spanwise P_T distribution of the *DIST* case along the diffuser centerline. The P_T profile is highly nonuniform at the diffuser inlet, and very little change is noticed in the semi-vaneless region. However, downstream of the throat, P_T becomes much more uniform across the span. Figure 5-4 shows that further downstream, P_T increases at those spanwise locations in which P_T was relatively low at the inlet, while P_T decreases at those locations in which P_T was high at the inlet. This result is very similar to that observed for the *NOMINAL* case in Figure 5-2; however, the effects are more pronounced in the *DIST* case in which high inlet distortion is present. The behavior indicates a work transfer from high P_T regions of the flow to low P_T regions; the more energetic fluid pulls the less energetic fluid through the diffuser channel via shear forces.

Comparison Summary

The comparison outlined above has indicated that, independent of the level of inlet axial distortion present, flow field distributions far downstream in the vaned diffuser channel are quite similar. Figure 5-5 shows the blockage distribution along the diffuser centerline from inlet to exit. For each case, blockage increases within the semi-vaneless region due to the effect of the adverse pressure gradient (recall Section 4.1.1). Previous theories have assumed that this blockage increase caused reduced channel pressure recovery, an assumption which is disproved in Chapter 4. Immediately after the throat, the blockage begins to decrease; this decrease is much stronger for the case of high inlet distortion. Near the end of the diffuser channel, the blockage is nearly equal in both cases, indicating near-complete attenuation of the inlet distortion.

The computed results appear to agree with the experimental results of Dutton et al. [15] and Yoshinga et al. [34] - inlet axial distortion is largely mixed out within the vaned diffuser channel. However, the distortion is not mixed out within the semi-vaneless region

of the diffuser; this is in contrast to the explanation put forward by Filipenco [18]. Rather, significant mixing is seen to begin immediately after the throat and continues along the diffuser channel.

5.2.2 Flow Processes Responsible for Distortion Attenuation

The previous section described the behavior of an inlet flow nonuniformity within the straight-channel diffuser. The flow angle and total pressure nonuniformities are significantly reduced within the diffuser channel, and the results presented indicate that viscous work transfer within the diffuser may contribute to this distortion attenuation.

The theories of Filipenco [18] and Dalbert et al. [4] indicate that in the presence of either a shear flow or a casing boundary layer, a secondary flow field develops in the diffuser passage which can result in the transport of high momentum flow to regions of low momentum, thus enhancing the mixing process within the diffuser. The computed result can be further examined to determine if such a secondary flow field contributes to the mixing process. Figure 5-6 shows P_T contours and cross-flow velocity vectors at the throat plane (normal to the diffuser centerline) for the *DIST* case with high inlet distortion. The P_T contours (high P_T is shown in white) show the strong flow nonuniformity present at the diffuser throat. The velocity vectors indicate the extent of the secondary flow field at the throat plane of the diffuser; the secondary velocity is 3% to 5% of the total velocity. Figure 5-7 and Figure 5-8 show the similar P_T contours and cross-flow velocity vectors at 22.9% and 57.5% of the diffuser centerline, respectively. The P_T contours indicate that the nonuniformity has decreased downstream. The velocity vectors indicate that the secondary flow has decreased to 1% of the total velocity at 57.5% of the diffuser centerline.

A strong secondary flow will contribute to mixing by transporting fluid, thereby changing the direction of flow field gradients. As can be seen from comparing Figure 5-6 and Figure 5-8, the P_T gradient does not change direction downstream in the diffuser channel: high P_T remains in the hub-pressure side corner and low P_T remains in the shroud-suction side corner. This indicates that the secondary flow field is weak, and does not contribute significantly to the mixing of the nonuniformity in the downstream channel. The dominant

cause of the mixing must be the viscous work transfer described in Section 5.2.1.

5.2.3 Effect of Work Transfer

Once work transfer has been identified as the driver for mixing within the diffuser, it is necessary to describe the effect this transfer has on the fluid mechanics of the diffuser. Figure 5-9 shows the static pressure contours for the low and high inlet distortion cases at $\hat{\alpha}_1 = 68°$, near the design point. As described in detail in Section 5.2.1 the inlet flow profiles of these two cases are very different; however, as shown in Figure 5-9, the static pressure distributions and Cp^{Ψ}_{1-2} are very similar. The question arises as to how such different inlet flow profiles may produce the same performance.

Separation off of Suction Vane Surface

Prior to answering such a question, it is necessary to examine the mechanics of flow separation in the diffuser. At very high flow angles, the inlet flow vector is poorly aligned with the diffuser vane, leading to separation off of the suction surface of the vane. This behavior can be seen in Figure 5-10, which shows the static and midspan total pressure contours of an off-design case from the *NOMINAL* study with $\hat{\alpha}_1 = 71.07°$. The static pressure contours show that overall pressure recovery is quite low due to poor channel performance. The total pressure contours indicate that the poor channel pressure rise is due to a massive separation observed off of the suction surface of the vane, which results in substantial low-momentum flow and reduces the effective diffuser exit area. While the momentum-averaged inlet flow angle for this case is $\hat{\alpha}_1 = 71.07°$, the local inlet flow angle across the span varies from 69.80° at the core to 74.88° near the casing. It is apparent that such a misaligned flow angle distribution will produce flow separation.

Separated Flow Reattachment Due to Work Transfer

Returning now to the highly distorted, near-design *DIST* case studied earlier in the chapter, it can be seen in Figure 5-3 that the local inlet flow angle varies from 63.60° to 83.30°. At some spanwise locations, local flow angles exist which are much larger than those flow

angles which were found to produce the massive flow separation shown in Figure 5-10. It has been previously been assumed [5] that such local flow angle misalignments produce localized stall regions which significantly reduce overall Cp. Bammert et al. [1] even designed a vaned diffuser with twisted blades to accept severely distorted inlet flow, and to reduce the effect of these anticipated localized stall regions.

In order to examine the effect of the highly distorted inlet profile on diffuser fluid dynamic processes, Figure 5-11 shows the total pressure contours at different spanwise locations near the hub, midspan, and shroud of the diffuser. Near the hub and midspan, where local inlet flow angles are below 70.0°, P_T contours show very little separation and loss off of the suction blade surface. Flow through the channel at these spanwise locations is fully developed and total pressure decreases along the channel.

Near the shroud, where local inlet flow angles approach 80.0°, the total pressure contours show a separation bubble on the suction surface near the blade leading edge. However, despite the large flow angle misalignments, this separation bubble never develops into the full channel stall which is observed in Figure 5-10. In addition, P_T along the shroud increases downstream of the channel throat. This P_T increase is due to the work transfer from the energetic hub and midspan regions to the shroud. As a result of the work transfer, the shroud flow is energized, and the separation bubble does not develop into localized channel stall. Flow at the exit of the diffuser channel does not suffer the high blockage associated with full channel stall, and good pressure recovery is thus preserved.

5.3 Conclusions and Implications

It is believed that the geometry of the tested vaned diffuser is such that the effect of work transfer can significantly affect the fluid mechanic processes in the diffuser. The ratio of length, L, to axial depth, b, of the tested diffuser is sufficiently large (L/b = 15.3) to allow inlet axial distortion to mix out due to viscous shear between axial fluid layers. This work transfer has been shown to prevent localized vane stall near the casing, and thus preserve channel pressure rise.

The results presented indicate that the vaned diffuser need not be designed specifically to accept inlet flow nonuniformity. Localized vane stall is prevented by work transfer across the diffuser span, reducing the need for twisted vanes which are tailored for specific flow vector distributions. Untwisted blades provide acceptable resistance to inlet axial distortion, and thus preserve good pressure recovery. Coupled with their simplicity in design and manufacture, untwisted vanes are an attractive alternative for the diffuser designer.

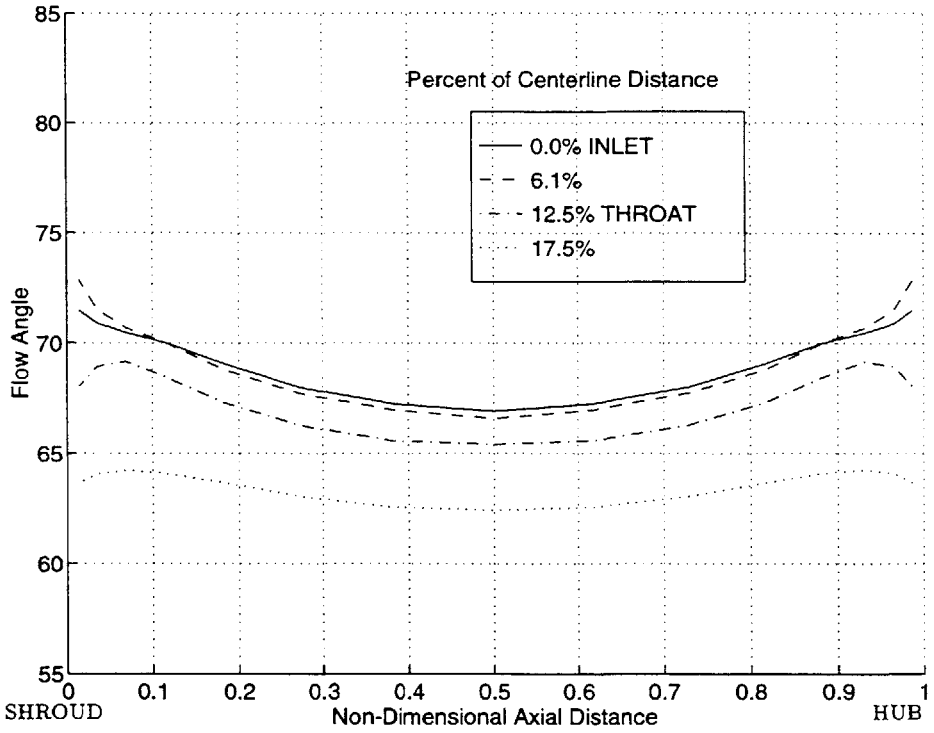

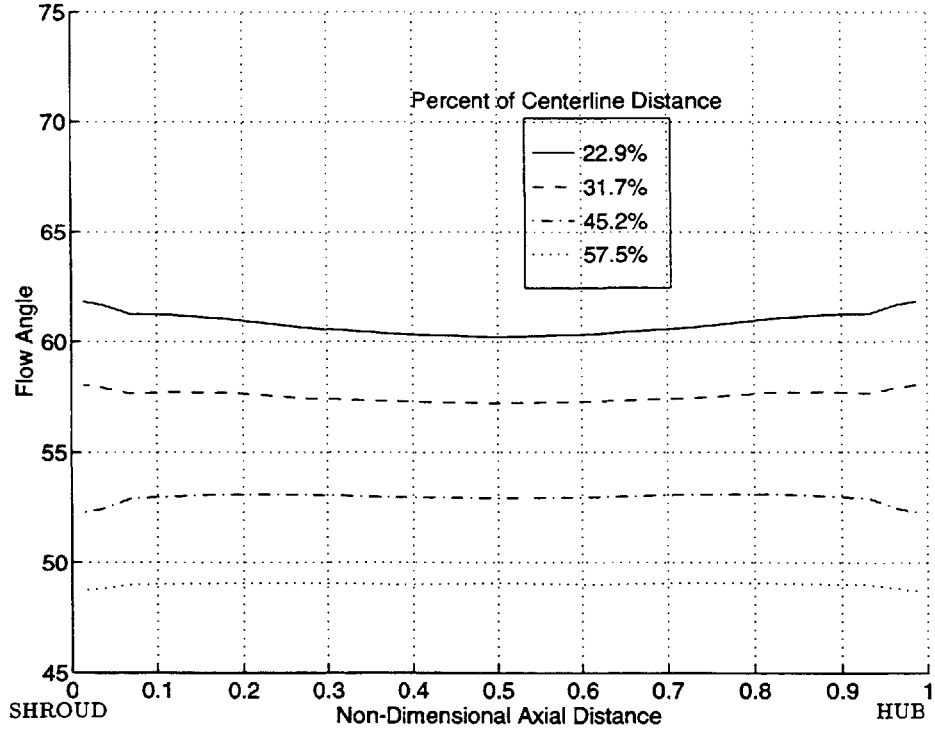

Figure 5-1: Spanwise Flow Angle Distributions Along the Centerline of the Straight-Channel Diffuser; Low Inlet Distortion.

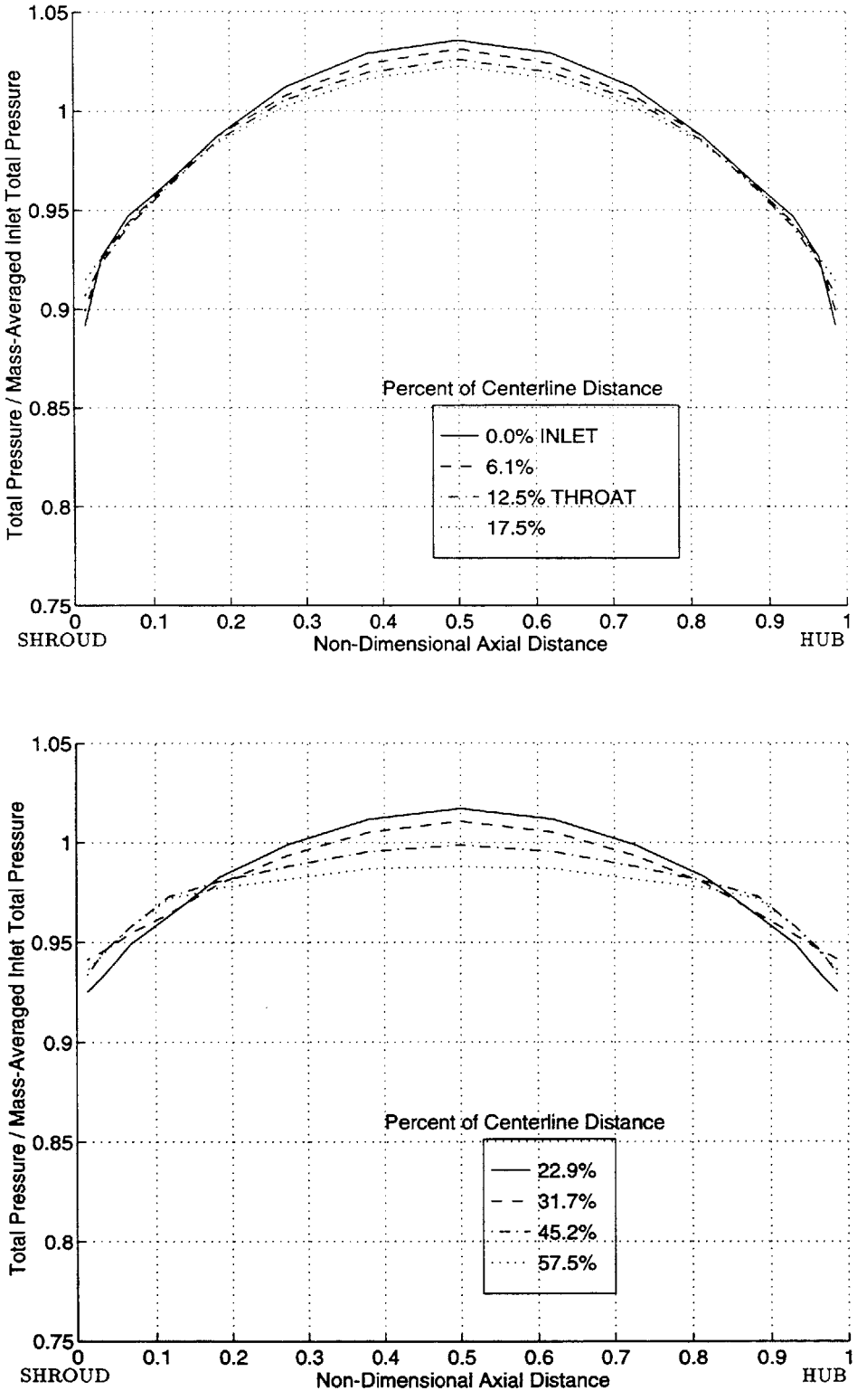

Figure 5-2: Spanwise Total Pressure Distributions Along the Centerline of the Straight-Channel Diffuser; Low Inlet Distortion.

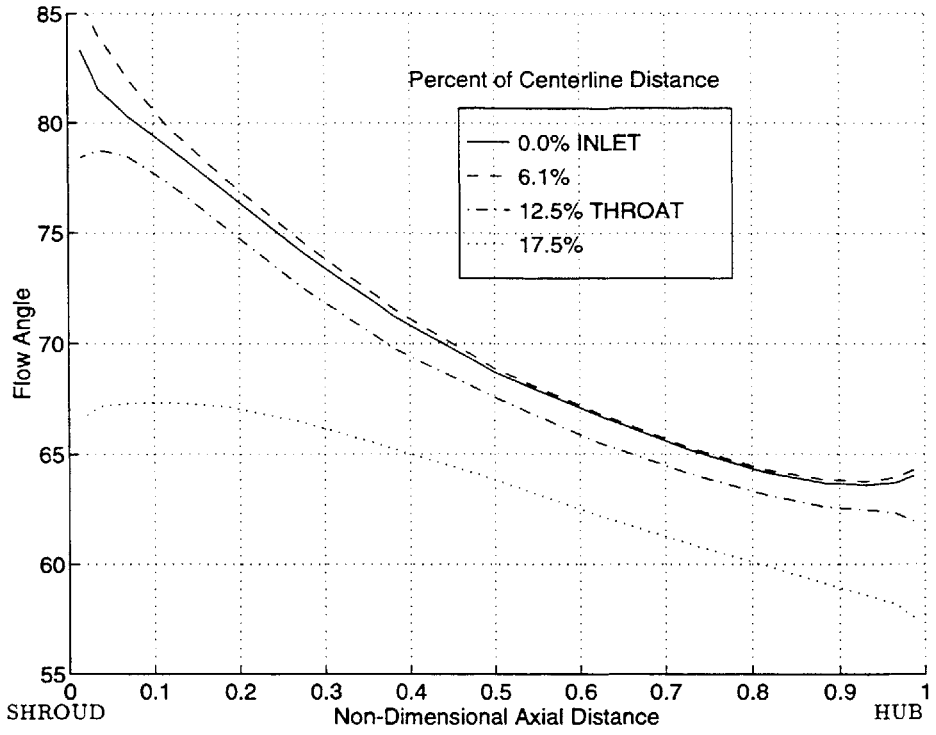

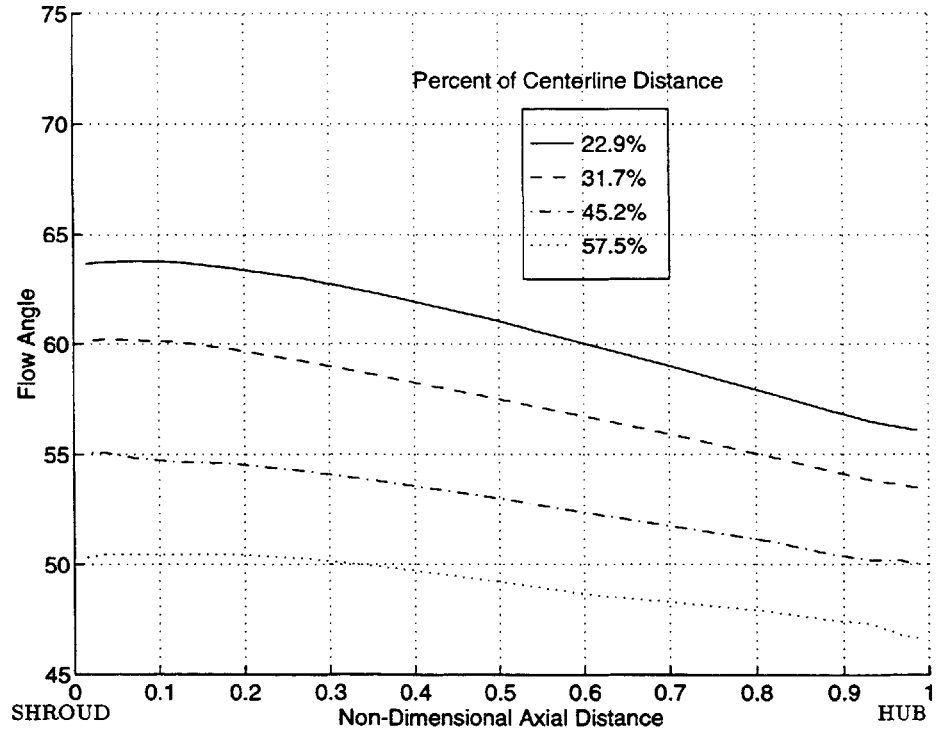

Figure 5-3: Spanwise Flow Angle Distributions Along the Centerline of the Straight-Channel Diffuser; High Inlet Distortion.

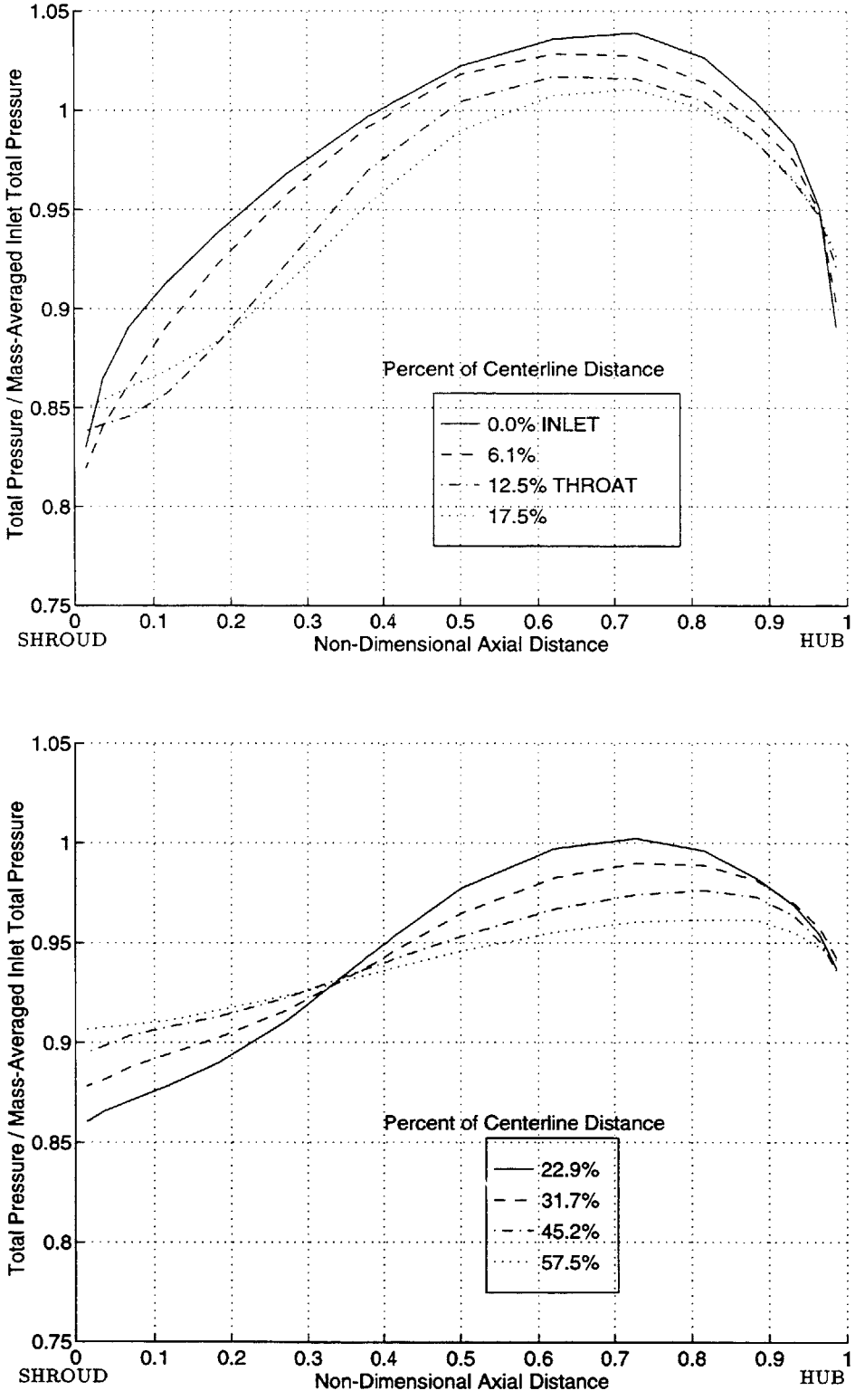

Figure 5-4: Spanwise Total Pressure Distributions Along the Centerline of the Straight-Channel Diffuser; High Inlet Distortion.

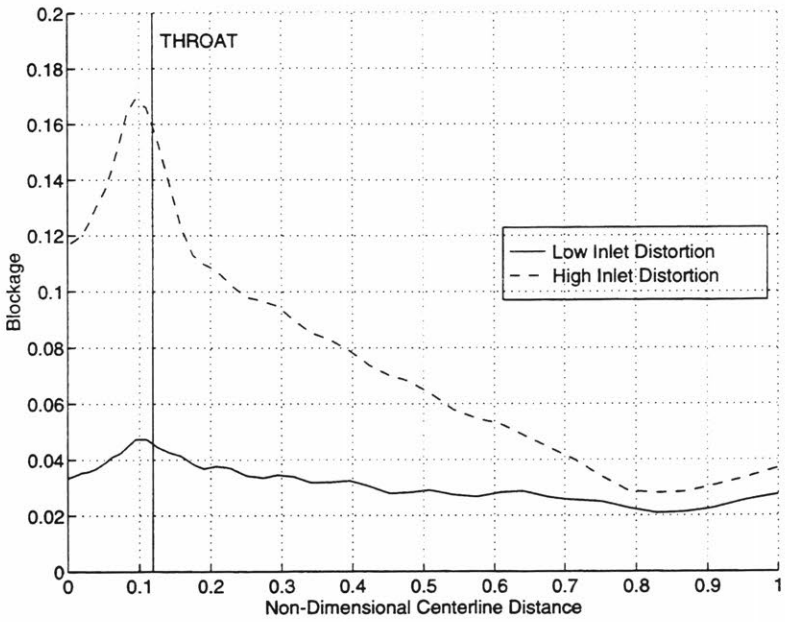

Figure 5-5: Blockage Distribution Along the Centerline of the Straight-Channel Diffuser; Low and High Inlet Distortion.

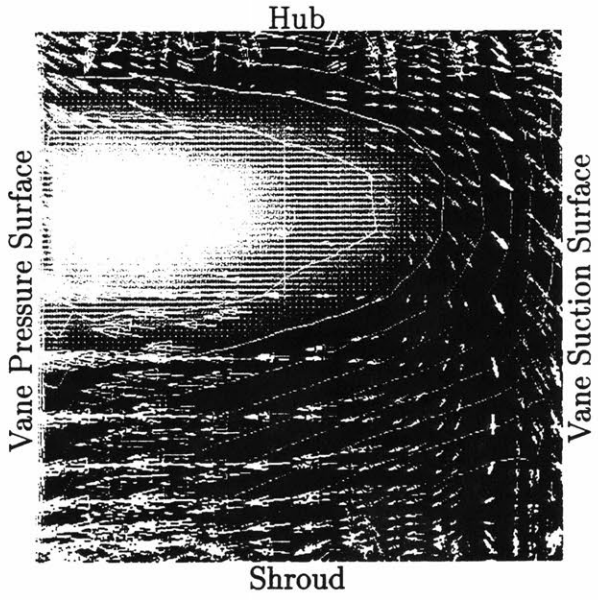

Figure 5-6: P_T Contours (High P_T in White) and Cross-Flow Velocity Vectors at Normal Plane (scale: $2 \times \mathcal{AS}$); 12.5% (THROAT) of the Diffuser Centerline.

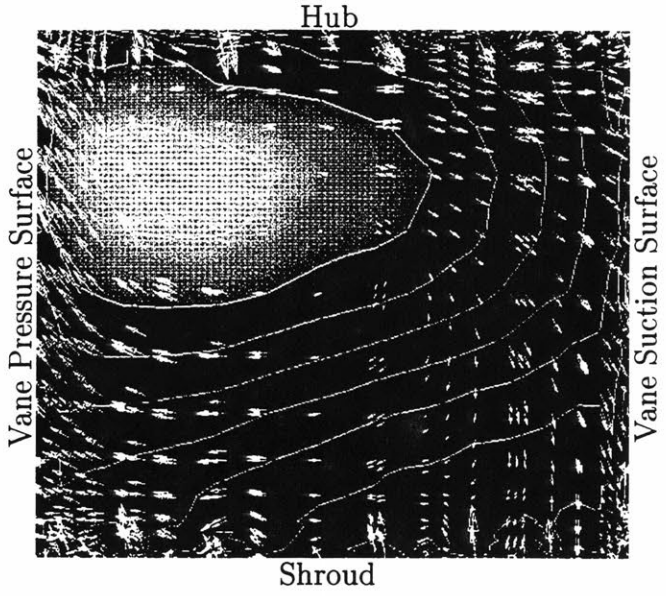

Figure 5-7: P_T Contours (High P_T in White) and Cross-Flow Velocity Vectors at Normal Plane (scale: $2 \times AS$); 22.9% of the Diffuser Centerline.

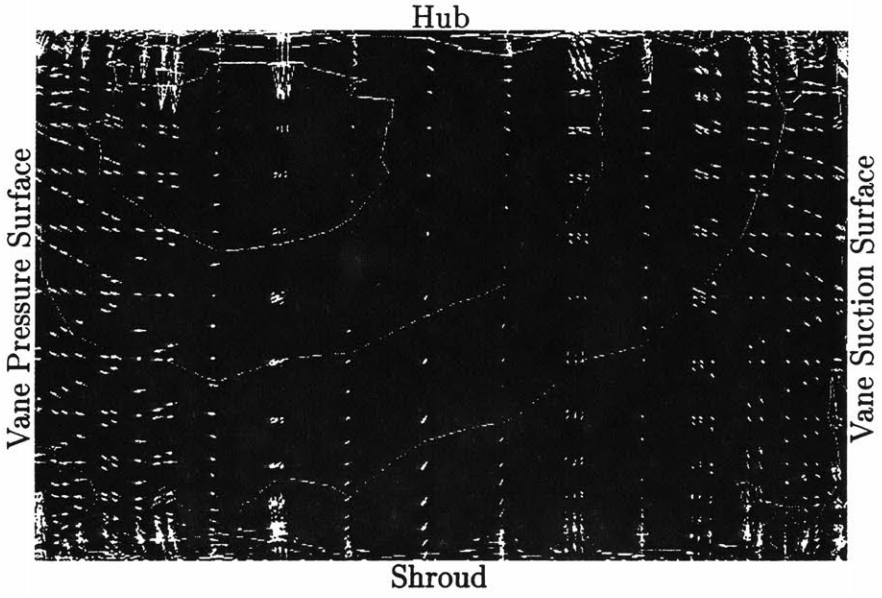

Figure 5-8: P_T Contours (High P_T in White) and Cross-Flow Velocity Vectors at Normal Plane (scale: $2 \times AS$); 57.5% of the Diffuser Centerline.

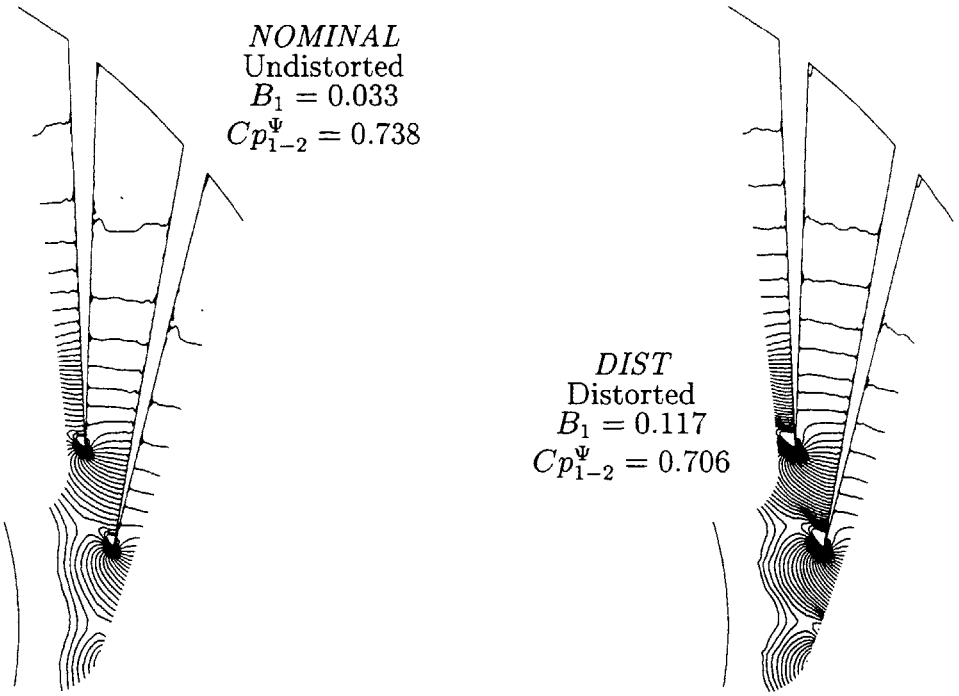

Figure 5-9: Static Pressure Contours; Undistorted and Distorted Cases at Near-Design Operating Point ($\hat{\alpha}_1 = 68°$).

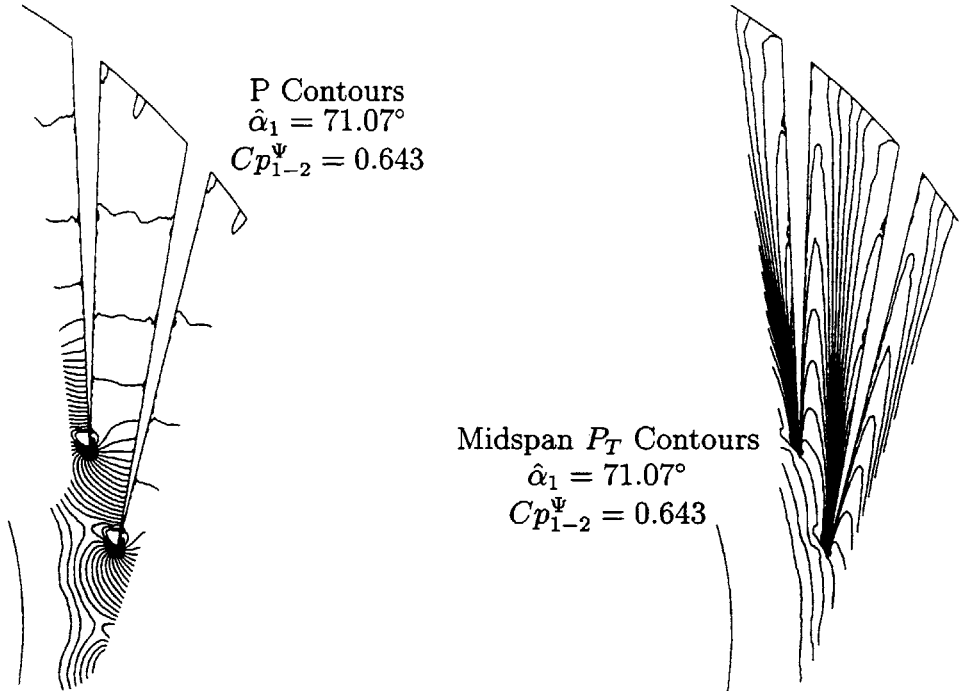

Figure 5-10: P and Midspan P_T Contours for a Case with Separated Channel Flow.

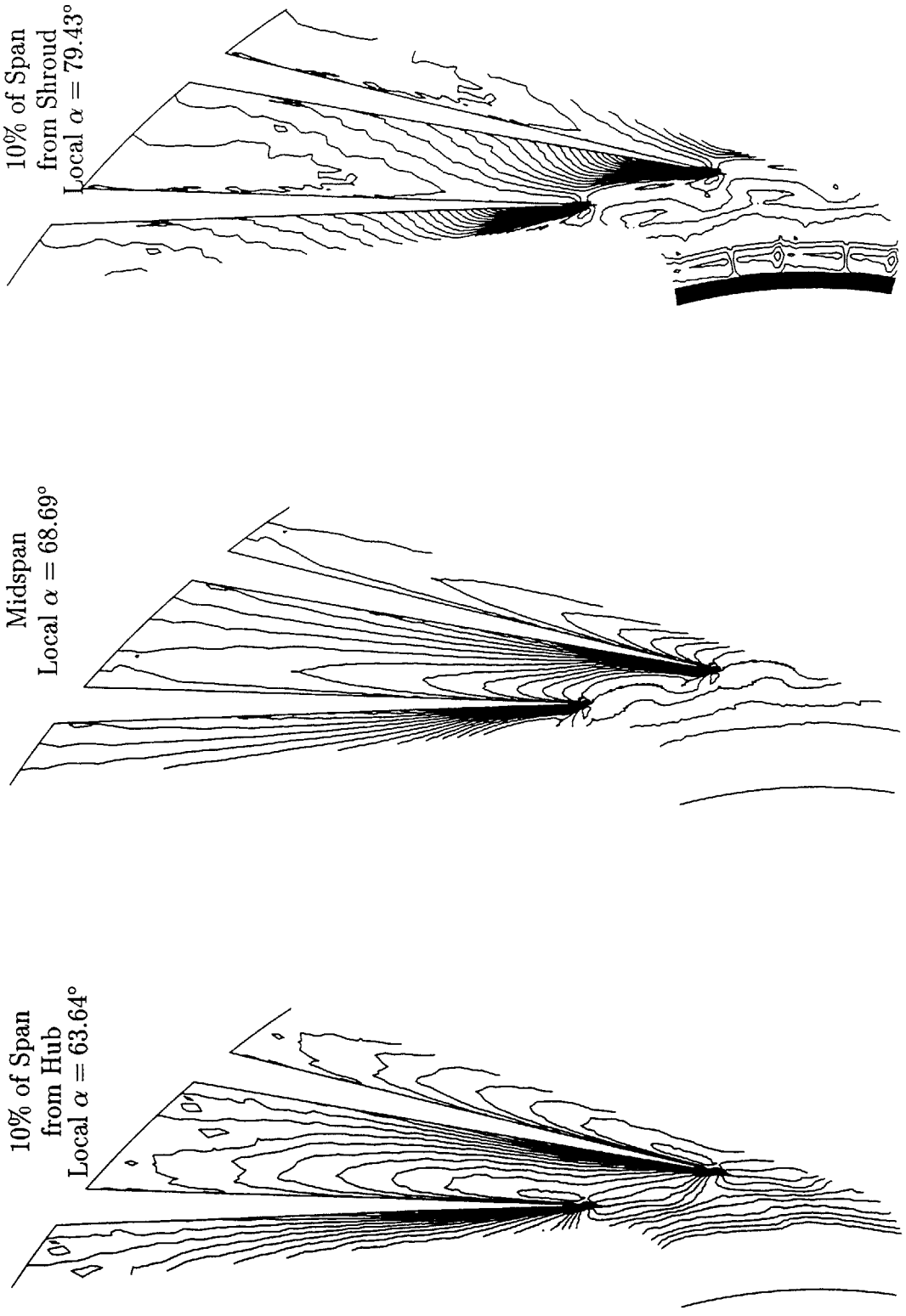

Figure 5-11: Total Pressure Contours at Different Spanwise Locations for a Near-Design Case ($\hat{\alpha}_1 = 68°$) with High Inlet Distortion.

Chapter 6

Summary

A computational investigation has been undertaken to elucidate the effects of inlet flow conditions on straight-channel diffuser performance; this includes addressing the role of inlet flow blockage and flow alignment on pressure recovery. This chapter provides an overview of the research contributions derived from the computed result, and explains the implications of these contributions in radial vaned diffuser design. Finally, recommendations for further study are outlined.

6.1 Overview of Research Contributions

The research contributions from this work are as follows:

- A three-dimensional Navier-Stokes solver was found to adequately model the experimentally measured result of Deniz [11]. This gives a certain degree of confidence in the use of such a code for the computational investigation of flow in vaned diffusers.
- Contrary to established view, excellent semi-vaneless pressure recovery *does not* necessarily result in poor channel performance in a straight-channel diffuser. The computed result shows that the throat blockage created in the semi-vaneless region does not strongly affect the downstream channel performance.

- Channel performance is primarily dependent on throat flow angle alignment with the geometric channel centerline angle. Flow angle misalignment causes premature flow separation off of the vane suction/pressure surfaces, thereby decreasing pressure recovery.

- Because the ratio of channel length to axial depth of the tested diffuser is sufficiently large, overall diffuser performance is insensitive to severe inlet axial distortion. Work transfer energizes regions of high flow angle misalignment, causing local separation bubbles to reattach to the vane suction surface, thus preserving diffuser performance.

6.2 Implications in Radial Vaned Diffuser Design

The fluid behavior observed in the computed result was then examined for possible application towards vaned diffuser design methods. Contributions to vaned diffuser design include the following:

- By sculpting the vane suction surface within the semi-vaneless region, a designer can adjust the geometric channel centerline angle, which controls the operating point at which channel performance is optimized. By changing the location of optimum Cp_{th-2}, the vaned diffuser may be designed to deliver good performance over a fairly wide flow range, or it may be tailored to deliver excellent performance over a more narrow range.

- Axially twisted vane designs which are tailored for specific inlet flow vector distributions may be unnecessary because the performance of a straight-channel diffuser with untwisted vanes has been found to be largely insensitive to inlet axial distortion. In addition, the use of untwisted blades reduces the complexities involved in design and manufacture.

6.3 Recommendations for Future Study

While the contributions and implications delineated above are significant, much additional insight may be gleaned from continued investigation of related topics. Additional research is recommended in the following areas:

- The fluid mechanics of the semi-vaneless and throat regions of a vaned diffuser should be experimentally investigated in order to validate the significant findings of the computed result. Fradin & Janssens [19] used the Laser-Two-Focus Velocimeter to investigate the flow angle and Mach number distribution inside a vaned diffuser. A similar experiment could investigate the effect of operating point on flow angle behavior in the diffuser throat. In addition, velocity measurements within the diffuser channel could yield information concerning momentum transfer across the diffuser span.

- The computed result outlines the fluid mechanics associated with inlet axial distortion at a near-design point. It is of interest to determine if the conclusions developed at design point are also true at off-design flow. Further investigation of the *DIST* studies at $\hat{\alpha}_1 = 66°$ and $70°$ are recommended.

- The computed result suggests the use of camber in the semi-vaneless region of a vaned diffuser in order to control performance and flow range. Complications with this design are briefly outlined, but an in-depth study of the effect of inlet region geometry is lacking. A computational investigation of the effect of a cambered leading-edge on pressure rise and operating range is recommended.

Bibliography

[1] Bammert, K., Jansen, M., Rautenberg, M., *On the Influence of the Diffuser Inlet Shape on the Performance of a Centrifugal Compressor Stage*, ASME Paper #83-GT-9, 1983.

[2] Cumpsty, N.A., Private Communication, 1996.

[3] Cumpsty, N.A., *Compressor Aerodynamics*, Longman Scientific & Technical, 1989.

[4] Dalbert, P., Gyarmathy, G., Sebestyen, A., *Flow Phenomena in a Vaned Diffuser of a Centrifugal Stage*, ASME Paper #93-GT-53, 1993.

[5] Dawes, W.N., *A Simulation of the Unsteady Interaction of a Centrifugal Impeller with its Vaned Diffuser: Flows Analysis*, ASME Paper #94-GT-105, 1994.

[6] Dawes, W.N., *The Practical Application of Solution-Adaption to the Numerical Simulation of Complex Turbomachinery Problems*, Prog. in Aerospace Sci., Vol. 29, 1992, pp. 221-269.

[7] Dawes, W.N., *The Simulation of Three-Dimensional Viscous Flow in Turbomachinery Geometries Using a Solution-Adaptive Unstructured Mesh Methodology*, ASME Paper #91-GT-124, 1991.

[8] Dawes, W.N., *The Development of a Solution-Adaptive 3-D Navier-Stokes Solver for Turbomachinery*, AIAA-91-2469, 1991.

[9] Dean, R.C., *The Fluid Dynamic Design of Advanced Centrifugal Compressors*, Technical Note TN-180, Creare Inc.,Hanover, N.H., 1973.

[10] Dean, R.C., Senoo, Y., *Rotating Wakes in Vaneless Diffusers*, ASME Journal of Basic Engineering, September, 1960.

[11] Deniz, S., *Effects of Inlet Flow Field Conditions on the Performance of Centrifugal Compressor Diffusers*, Massachusetts Institute of Technology, Department of Aeronautics & Astronautics, Gas Turbine Laboratory, December, 1996.

[12] Deniz, S., Private Communication, 1996.

[13] Dolan, F.X., Runstadler, P.W., *Pressure Recovery Performance of Conical Diffusers at High Subsonic Mach Numbers*, Technical Report CR-2299, NASA, August, 1973.

[14] Dong, Y., Private Communication, 1996.

[15] Dutton, J.C., Piemsomboon, P., Jenkins, P.E., *Flowfield and Performance Measurements in a Vaned Radial Diffuser*, Journal of Fluids Engineering, Vol. 108, June, 1986, pp. 141-147.

[16] Eckardt, D., *Untersuchung der Strahl/Totwasserströmung hinter einem hochbelasteten Radialverdichterlaufrad*, Dissertation, R.W. Technische Hochschule Aachen, Germany, 1977.

[17] Ensenat, S., *Comparison of Numerical Methods to Calculate Diffuser Performance*, Massachusetts Institute of Technology, Department of Aeronautics & Astronautics, Research Report, May, 1996.

[18] Filipenco, V.G., *Experimental Investigation of Flow Distortion Effects on the Performance of Radial Discrete-Passage Diffusers*, Massachusetts Institute of Technology, GTL Report #206, Cambridge, MA (PhD. Thesis), 1991.

[19] Fradin, C., Janssens, G., *Detailed Measurements of the Flow Field at the Outlet of a Backswept Transonic Centrifugal Impeller Equipped with a Vaned Diffuser*, Fourth International Symposium, ASME Cogen-Turbo, New Orleans, 1990, pp. 249-254.

[20] Japikse, D., *Centrifugal Compressor Design and Performance*, Concepts ETI, Inc., 1996.

[21] Johnston, J.M., *Stall Onset Observations of a Discrete Passage Diffuser*, Massachusetts Institute of Technology, GTL Report #217, Cambridge, MA (S. M. Thesis), 1993.

[22] Kano, F., Tazawa, N., Fukao, Y., *Aerodynamic Performance of Large Centrifugal Compressors* ASME Paper #82-GT-17, 1982.

[23] Kenny, D.P., *A Comparison of the Predicted and Measured Performance of High Pressure Ratio Centrifugal Compressor Diffusers*, ASME Paper #72-GT-54, 1972.

[24] Krain, H., *A Study on Centrifugal Impeller and Diffuser Flow*, ASME Paper #81-GT-9, 1981.

[25] Liang, Y., *Investigation of Inlet and Entry Region Characteristics on the Discrete Passage Diffuser Pressure Rise Performance*, Massachusetts Institute of Technology, Department of Aeronautics & Astronautics, S.M. Thesis, 1994.

[26] Morishita, E., *Centrifugal Compressor Diffusers*, S. M. Thesis, University of Cambridge (England), Department of Engineering, 1982.

[27] Phillips, R.A., *Distribution of Computation in a Multiprocessor System*, Massachusetts Institute of Technology, Department of Electrical Engineering & Computer Science, S.M. Thesis, 1988.

[28] Reneau, L.R., Johnston, J.P., Kline, S.J., *Performance and Design of Straight, Two-Dimensional Diffusers*, Journal of Basic Engineering, Trans. ASME, Vol. 89, March, 1967, pp.141-150.

[29] Rodgers, C., *Compact Diffusers for Small Transonic Compressors*, AGARD Meeting on Technology Requirements for Small Gas Turbines, Paper #19, AGARD-CP-537, March, 1994.

[30] Runstadler, P.W., Dolan, F.X., Dean, R.C., *Diffuser Data Book*, Technical Note TN-186, Creare Inc., Hanover, N.H., 1975.

[31] Runstadler, P.W., Dolan, F.X., *Further Data on the Pressure Recovery Performance of Straight-Channel, Plane-Divergence Diffusers at High Subsonic Mach Numbers*, ASME Paper #73-FE-5, 1973.

[32] Tan, C.S., Greitzer, E.M., *Impact of Unsteady Impeller-Diffuser Interactions on Centrifugal Compressor Performance*, Massachusetts Institute of Technology, Department of Aeronautics & Astronautics, Gas Turbine Laboratory, Research Program Proposal, 1993.

[33] Traupel, W., *Thermische Turbomaschinen*, Band 1, Auflage 3, Springer Verlag, 1977.

[34] Yoshinaga, Y., Kobayashi, H., Kaneki, T., *A Study of Aerodynamic Performance of Diffusers for Centrifugal Compressors*, Bulletin of JSME, Vol. 28, No. 242, August, 1985, pp. 1651-1658.